Acta Universitatis
Lappeenrantaensis
807

Mohammad Dabiri

THE LOW-CYCLE FATIGUE OF S960 MC DIRECT-QUENCHED HIGH-STRENGTH STEEL

Mohammad Dabiri

THE LOW-CYCLE FATIGUE OF S960 MC DIRECT-QUENCHED HIGH-STRENGTH STEEL

Thesis for the degree of Doctor of Science (Technology), to be presented with due permission for public examination and criticism in the lecture room 2303 at Lappeenranta University of Technology, Lappeenranta, Finland on the 18th of October, 2018, at noon.

Acta Universitatis
Lappeenrantaensis 807

Supervisor Professor Timo Björk
School of Energy Systems
Lappeenranta University of Technology
Finland

Reviewers Professor Xiao-Ling Zhao
Department of Civil Engineering
Monash University
Australia

Associate Professor Robert Basan
Department of Mechanical Engineering Design
University of Rijeka
Croatia

Opponent Associate Professor Zuheir Barsoum
Department of Aeronautical and Vehicle Engineering
KTH Royal Institute of Technology
Sweden

ISBN 978-952-335-257-5
ISBN 978-952-335-258-2 (PDF)
ISSN-L 1456-4491
ISSN 1456-4491

Lappeenrannan teknillinen yliopisto
LUT Yliopistopaino 2018

Abstract

Mohammad Dabiri

THE LOW-CYCLE FATIGUE OF S960 MC DIRECT-QUENCHED HIGH-STRENGTH STEEL

Lappeenranta 2018
58 pages
Acta Universitatis Lappeenrantaensis 807
Diss. Lappeenranta University of Technology
ISBN 978-952-335-257-5, ISBN 978-952-335-258-2 (PDF), ISSN-L 1456-4491, ISSN 1456-4491

Demanding strength, manufacturability and critical weight limitations are generally the main criteria in the design and fabrication of structural components. The emergence and development of ultra-high and high-strength materials, especially steels benefiting from an excellent high strength to weight ratio, along with their acceptable manufacturability, led to the special role that these materials play in the industry. Although they are so promising for components that experience static loading conditions, their dominant field of application (i.e. mobile machineries and equipment) imposes fluctuating service loads on them, making these structural members susceptible to fatigue failure. In addition, due to the inevitable presence of stress raisers and notches in real components, the high-strength steels, with their high-notch sensitivity, could suffer more compared with other commercial low- and medium-strength steels.

In this study a high-strength steel S960 MC (direct-quenched) is selected for a comprehensive fatigue analysis under constant amplitude loading. The study covers the aspects of microstructural analysis, experimental tests and numerical simulations. The microstructural investigations are performed in order to first characterize the material in question and then analyse the fatigue fracture surfaces. The result of measurements is also used in numerical simulations.

Experiments, such as tensile and low-cycle fatigue tests, are conducted on plain specimens. Using the experimental strain-life curve as the reference, different methods available for the estimation of this important curve are evaluated and a new model, based on artificial neural networks, is proposed. The application of this technique is extended to the estimation of stress concentration factors in butt- and T-welded joints, resulting in models with higher accuracy compared with available parametric equations. The model is also able to explicitly take in to account the effect of axial misalignment (in butt-welded joints) and undercut (in T-welded joints).

Notched specimens made of the same material as that in question are also investigated in the present study. Common analytical approaches, such as Neuber’s rule and the strain energy density method, are used in order to compare their estimations with the experiments and elastoplastic finite element simulations. An approach based on the theory of critical distances (TCD) is also utilized, yielding the best fatigue life

estimations when compared to other approaches. In order to investigate the microstructural effects on this method and mainly on its parameter (the material characteristic length), the crystal plasticity formulation is used to model the microstructural heterogeneities at the critical zone of the notch root. It was interesting to observe that the crystal plasticity finite element (CPFE) model is also able to be used coupled with the TCD concept in order to estimate the material's characteristic length and to perform the notch fatigue analysis. This is a valuable finding, showing the possibility of simultaneously utilizing the elastoplastic TCD with CPFE models, which are so demanding and extensively used in multiscale modelling of fatigue and failure of metals.

Keywords: low-cycle fatigue, high-strength steel, notches, weld, crystal plasticity, finite element, artificial neural network

Acknowledgements

I would like to acknowledge and express my heartfelt gratitude to the following people:

- To my supervisor, Professor Timo Björk, for his continual support and trust
- To Professor Zuheir Barsoum, for kindly agreeing to act as the opponent
- To Professor Xiao-Ling Zhao, for his time and consideration, acting as the first reviewer of this dissertation and providing valuable comments and corrections
- To Professor Robert Basan, for kindly providing me with access to the MATDAT (Materials Properties Database) and acting as the second reviewer of this dissertation
- To Professor Gabriel Potirniche, for his guidance and support during my research visit at the University of Idaho, USA
- To Matti Lindroos, Matti Isakov and Tuomas Skriko, for their significant succour and contributions
- To my colleagues at the Steel Structures Laboratory
- To Peter Jones, for his invaluable assistance with language editing of all the publications included in this manuscript.

Finally, yet importantly, I am grateful to my family and beloved wife, Helia; without her this journey would not have reached an end.

Mohammad Dabiri
May 2018
Lappeenranta, Finland

Contents

List of publications

This thesis is based on the following peer-reviewed journal articles, referred to as *publications* hereafter and introduced in the text by the letter *P* combined with a roman numeral (P-I to P-V). The rights have been granted by publishers to include the articles in the printed form of this dissertation.

I. Dabiri, M., Isakov, M., Skriko T. & Björk, T., 2017. Experimental fatigue characterization and elasto-plastic finite element analysis of notched specimens made of direct-quenched ultra-high-strength steel. *Proceedings of the Institution of Mechanical Engineers, Part C: Journal of Mechanical Engineering Science*, 231(22), pp. 4209–4226.

II. Dabiri, M., Ghafouri, M., Rohani Raftar H. R. & Björk, T., 2018. Evaluation of strain-life fatigue curve estimation methods and their application to a direct-quenched high-strength steel. *Journal of Materials Engineering and Performance*, 27(3), pp. 1058–1072.

III. Dabiri, M., Ghafouri, M., Rohani Raftar H. R. & Björk, T., 2017. Neural network-based assessment of stress concentration factor in a T-welded joint. *Journal of Constructional Steel Research*, 128, pp. 567–578.

IV. Dabiri, M., Ghafouri, M., Rohani Raftar H. R. & Björk, T., 2017. Utilizing artificial neural networks for stress concentration factor calculation in butt welds. *Journal of Constructional Steel Research*, 138, pp. 488–498.

V. Dabiri, M., Lindroos, M., Andersson, T., Afkhami, S., Laukkanen, A. & Björk, T., 2018. Utilizing the theory of critical distances in conjunction with crystal plasticity for low-cycle notch fatigue analysis of S960 MC high-strength steel. *International Journal of Fatigue*, 117, pp. 257–273.

P-I explains low-cycle fatigue tests that were conducted on plain and notched specimens along with the numerical simulation of cyclic stabilization and notch fatigue analysis by using the elastoplastic finite element method.

P-II investigates the approaches and models capable of estimating the strain-life fatigue curve under uniaxial constant amplitude cyclic loading. Approximations using the monotonic properties, models based on continuum damage mechanics and artificial neural networks (ANNs) are investigated and a new ANN-based model is proposed and implemented. The success of this model was an incentive to extend its usage in order to estimate the stress concentration factor of welded components.

P-III explains the usage of ANN-based models in estimation of stress concentration factor of fully penetrated T-welded joints under axial, bending and axial-bending loads.

The model successfully takes the undercut's effect into account in the calculation of the stress concentration factor.

P-IV explains the usage of ANN-based models in the stress concentration factor estimation of butt-welded joints in both single-V and double-V forms. The model explicitly considers the axial misalignment and shows higher accuracy compared to parametric equations.

P-V investigates the effect of introducing the microstructural heterogeneities on the estimation capability of the promising notch fatigue analysis method named the theory of critical distances (TCD). To this end, the integrated numerical model of crystal plasticity and finite elements is implemented and utilized to estimate the material characteristic length used for fatigue life estimation by the elastoplastic reformulation of TCD.

M. Dabiri was the principal planner, author and investigator of all these publications. M. Isakov and T. Skriko contributed to the experimental tests in P-I. M. Ghafouri and H. R. Rohani Raftar contributed to the numerical modelling and network implementations of P-II, P-III and P-IV. S. Afkhami contributed to the fracture surface analysis in P-V. M. Lindroos contributed to the numerical modelling in P-V. Other co-authors contributed by providing helpful comments.

Nomenclature

Latin alphabet

b	fatigue strength exponent
b_1 , b_2	slip hardening saturation coefficients
c	fatigue ductility exponent
C	material parameter
C_1 , C_2	material constants
C_{11}, C_{12}, C_{44}	elastic constants
d	kinematic parameter
D	damage variable
D_c	critical damage
D_N	damage corresponding to N cycles
D_0	initial damage
E	Young's modulus
h	reinforcement height
h_p	weld leg size
$h_1 - h_8$	interaction matrix coefficients
K	strength coefficient
k_f	fatigue notch factor
k_t	stress concentration factor
K'	cyclic strength coefficient
L	material characteristic length
n	strain hardening exponent
n'	cyclic strain hardening exponent
N	number of cycles
N_t	transition fatigue life
$2N_f$	reversals to failure
q	kinematic parameter
Q_1 , Q_2	softening parameters
r	weld toe radius
R	notch radius
S_e	endurance limit
t	plate thickness
t_p	attachment thickness
v	strain rate exponent
w	weld (attachment) width

Greek alphabet

β	elastoplastic tensor
δ	scale transition variable
$\Delta\varepsilon$	strain range
ε	strain

ε_f	true fracture strain
ε'_f	fatigue ductility coefficient
ε_0	threshold strain
$\overline{\varepsilon}$	equivalent strain
σ	stress
σ_f	true fracture strength
σ_u	ultimate tensile strength
σ_y	yield strength
σ'_f	fatigue strength coefficient
σ'_y	cyclic yield strength
τ	shear stress
τ_0	initial resolved shear stress
θ	flank angle

Superscripts

g	a term for a grain or phase
pl	plastic

Subscripts

a	amplitude
e	elastic
p	plastic

Abbreviation

AISI	American Iron and Steel Institute
ANN	Artificial neural network
ASTM	American Society for Testing and Materials
CDM	Continuum damage mechanics
CPFE	Crystal plasticity finite element
CSSC	Cyclic stress-strain curve
DIN	Deutsches Institut für Normung (German Institute for Standardization)
FE	Finite element
HB	Brinell hardness
HV	Vickers hardness
LCF	Low-cycle fatigue
LM	Line method
PM	Point method
RA	Reduction in area
SAE	Society of Automotive Engineers
SED	Strain energy density
SEM	Scanning electron microscope
SCF	Stress concentration factor
TCD	Theory of critical distances

1 Introduction

The development of direct quenching can be traced back to the late 1970s in Japan for plate production, and following this, the same process was applied in Europe to hot strip mill production (Kömi et al., 2016). By optimization of the chemical components and processing parameters, new types of steels with a variety of strength–ductility combinations were developed by this production process for a broad range of applications. Among those, the direct-quenched high-strength steels that benefited from the features of high strength and low weight, and from their forming ability, took the lead, especially in weight-critical constructions such as the structural members of mobile equipment (Ban & Shi, 2018). In this way (by direct quenching) not only a significant cut can be made in time and cost (as an alternative to the conventional quenched and tempered or thermomechanical rolling), but also its facilities can be used to produce microstructural constituents, not just martensite, which opens up possibilities for producing multiple constituent steels(Yoshie et al., 1992).

Almost all the structures made of direct-quenched high-strength structural steels are expected to undergo cyclic loads, making them susceptible to fatigue failure. Thus, the utilization of the increased strength of these steels presents challenges with respect to fatigue design (Kömi et al., 2016). In durability analysis and the design of components, knowledge of the relationship between stress and strain, and the fatigue life of the material used or to be used is a fundamental requirement. Experimental tests are invariably required to obtain the stress and strain relationship, which is unique for each material. The objective of such laboratory tests is to obtain information on the fatigue behaviour of small test specimens that can be used to simulate the behaviour of actual structures if tests on full-scale components are not practical. An approach that relates the failure life of a specimen to the constant amplitude strain range to which it is subjected is the strain-life (ε-N) approach. In this method, standard strain-controlled fatigue testing is performed on specimens of a specific material in order to evaluate the behaviour of the material when subject to fluctuating strain conditions. These tests attempt to simulate the magnitude and intensity of the strain fluctuations anticipated during service and the results are used to predict the fatigue strength of the material under the test conditions.

With respect to the fatigue properties of high-strength steels, they are superior to those of conventional structural steels with a moderate yield strength. However, geometrical discontinuities, such as notches, could significantly decrease their fatigue strength. In the literature, the term *notch* is used to refer to unavoidable geometric discontinuities in the design that act as stress raisers, such as holes, grooves, keyways and also local weld reinforcement and imperfections. This high notch sensitivity demands for a higher degree of precaution in the design and fatigue analysis of notched and welded components made of high-strength steels.

Similitude is assumed when the strain-based approach is used to perform fatigue strain analysis in localized regions in load-carrying components. The similitude concept states

that the cyclic response and fatigue damage accumulation of the material at the notch root is comparable to (that is, it has similitude with) the behaviour of an un-notched, axially loaded specimen in the same stress–strain states.

At highly stressed regions near a notch, plastic deformation is controlled by the surrounding elastic/pseudo-elastic matrix (Levkovitch et al., 2006); thus, a totally strain-controlled test can be considered a fair representation of the conditions experienced by the material in regions where significant localized plastic deformation is present. In addition, strain-controlled tests have gained increasing use in the determination of cyclic stress–strain curves for engineering alloys. This curve acts as a necessary part of the information required for many notch fatigue analysis methods. Although possible to obtain this stabilized response of the component by conducting the stress-controlled tests, because of the structural constraint of the material at fatigue-critical sites in real components, it seems appropriate to characterize the fatigue response of engineering materials on the basis of data obtained under strain-controlled cyclic loading (as a fully-constrained loading condition) rather than under stress-controlled cyclic loading (as a fully unconstrained loading condition). Therefore, each material should be tested and undergo the aforementioned experiments in order to be validated for applications exposed to cyclic loading.

In addition to the plain simple specimens mainly used in laboratory tests, the response of the component in the presence of notches and geometrical discontinuities should also be thoroughly investigated. Fatigue analysis approaches for notched components depend strongly on the stress–strain values for life assessment, in addition to the cyclic stress–strain curve (CSSC), and a number of approximate methods for estimating notch stresses and strains have been developed and proposed in the relevant literature. Moreover, advancement in computational capabilities has made the numerical methods a powerful technique for the fatigue analysis of components experiencing uniaxial and multiaxial conditions. Although successful in different aspects of components' life estimation from a fatigue point of view, the vastness of the proposals and methods in open literature can be devastatingly confusing for practitioners and design engineers interested in the most clear and straightforward approaches that have satisfactory accuracy. There is no need to mention the high complexity of some of the methods that makes them only applicable by experts, such as fatigue specialists, and not by accustomed practitioners and designers.

Furthermore, most of the empirical and numerical methods neither explicitly consider the heterogeneity of the material in microscale nor its effect on the macro-behaviour of the material. Materials have complex microstructures that determine their behaviour at the continuum level. One needs to understand the effect of those complexities in order to effectively predict the material's behaviour by following the dominant mechanisms at different length scales. These microstructural effects could also be of significant importance when the fatigue analysis is performed on notched specimens and components.

In the current study, investigation of the most common empirical, analytical and numerical methods for the fatigue analysis of plain and notched specimens under uniaxial constant amplitude loading are performed exclusively on the material under investigation. Different aspects from experimental tests and characterisations, approximations for strain-life curve estimation and notch fatigue analysis (including the available methods and new models proposed in the current study) are covered. The important concepts of the stress concentration factor (SCF) and misalignment vital for the fatigue analysis of welded components of mainly high-strength steels are scrutinized and new models are proposed.

1.1 The thesis's objectives and contribution to research

The importance of knowing the material response and its characteristics specifically under cyclic loading and subsequent fatigue failure (as one of the main failure mechanisms that occurs mainly in industrial applications of high-strength steels) acted as the principal incentive to study this particular direct-quenched type of high-strength steel and its response under low-cycle fatigue (LCF). The main goals and contributions can be divided into two categories, as follows:

I. New results through experimental tests and measurements

The detailed characterisation of the material under investigation was conducted by performing mechanical tests under monotonic and cyclic loads. Detailed microstructural measurements – such as optical microscopy, X-ray diffraction, scanning electron microscopy and electron backscatter diffraction analyses – were made in order to fully characterise the material in question besides providing the required data for the calibration of material parameters in constitutive equations, such as those of hardening rules and crystal plasticity. The notch fatigue analysis was also performed in an extensive way on this material, for the first time covering the most well-known analytical approaches besides the conventional elastoplastic finite element (FE) method and method of the theory of critical distances (TCD).

The material data obtained as the result of this research was added to MATDAT (Materials Properties Database) and indexed by the Data Citation Index (a part of Web of Science). There are also studies by the author (or studies to which the author contributed) of the effect of machining parameters on the surface residual stress of fatigue specimens, the plane stress fracture toughness measurements and on the dissimilar welds of S960 MC and duplex stainless steel, which are not included in the contents of the current thesis.

II. Novelties created through utilizing the mathematical and numerical techniques

In this aspect, the work contributed to the literature firstly by the evaluation of models based on artificial neural networks (ANNs) used in the estimation of strain-life fatigue curve. The limited proposals for the application of this technique for strain-life curve

estimation were reviewed and a new model was implemented. In addition, the configurations, such as butt- and T-welded joints, were simulated and used in the implementation of new ANN-based models for the estimation of SCFs. The proposed models showed the highest level of accuracy compared with the available parametric equations. Moreover, they have the ability to explicitly take the effects of undercut (in T-welded joints) and axial misalignment (in butt-welded joints) into account, which is not possible with the other equations.

The next contribution in this category would be the utilization of a coupled numerical model that is to be integrated with the elastoplastic reformulation of the TCD in a low-cycle regime. That is, the calibration process of the TCD, conducted in order to find the material characteristic length, was performed with a crystal plasticity finite element (CPFE) model instead of a conventional FE model.

1.2 Thesis outline

The contents of the thesis are categorized into six chapters, including this introduction chapter and the finalizing conclusion chapter. Each chapter that provides experimental or analytical results is concluded by a discussion section that fully explains the outcomes of the whole chapter, along with their related application to other sections. Therefore, there is no stand-alone discussion chapter and the thesis comes to an end with the finalizing summary and conclusion (Chapter 6). The manuscript is kept concise and at the introductory level, and no in-depth explanations are given. Appropriate referrals to the relevant publications (P-I to P-V) are made within the text in order that they may be consulted for detailed information regarding each section.

Chapter 2 describes the specifications of the material under investigation, along with the experimental tests, in order to characterize its mechanical behaviour and provide the essential data for tuning the material response in the models used in the subsequent sections. A study of the fracture surface of the specimens (plain and notched) in order to provide the information regarding their failure modes is also included in this chapter. Analysis of the plain specimens by numerical simulation of their stabilized cyclic response and the approximations and mathematical models used to estimate the strain-life fatigue curve of S960 MC are explained in Chapter 3. An extension of the applied mathematical technique (based on ANNs) used for the estimation of the SCFs of butt- and T-welded joints is described in Chapter 4. Finally, the study of notched specimens by analytical approximations, the elastoplastic FE method and the TCD are described in Chapter 5. This chapter also explains a modified numerical model which combines the elastoplastic reformulation of TCD with the concept of crystal plasticity. Chapter 6 gives the summary and concludes this manuscript. The findings of the current study are beneficial for design engineers working with this type of steel, in addition to researchers interested in the further development of the methods and proposals made here. Therefore, the suitable topics for the extension of this work that demand further investigation are also discussed and pointed out in the summary and conclusions

chapter. The overall outline of the thesis, showing its relation to each publication, is shown in Figure 1.1.

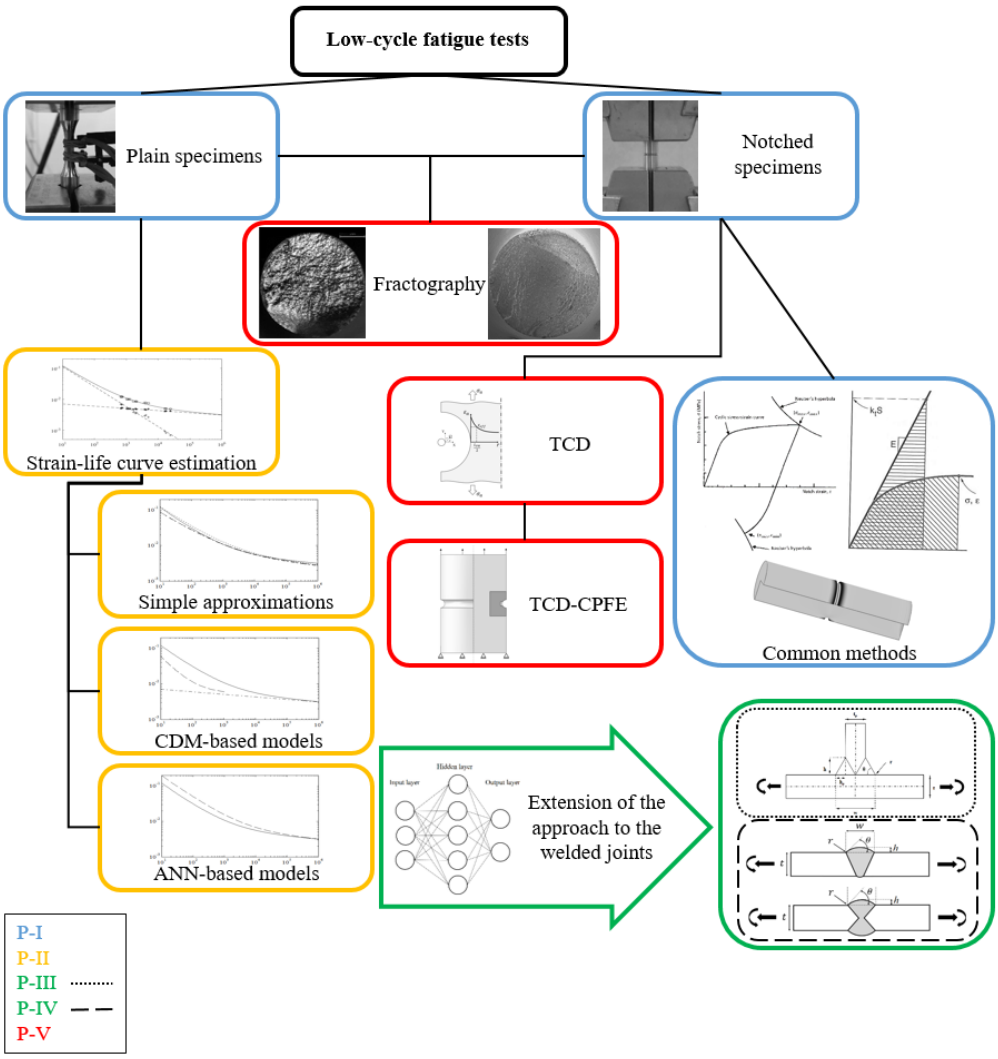

Figure 1.1: The thesis outline

2 Experiments

2.1 Material

A direct-quenched high-strength steel (S960 MC) is used in this study. This type of steel, unlike conventional quench-tempered steels, does not undergo a reheating stage after its final hot rolling process. Thus, contrary to quench-tempered steels, S960 MC does not necessarily experience austenite recrystallization since it is water quenched immediately after its final stage of hot rolling. The hot rolling process is carried out at a temperature at which austenite can be either recrystallized or non-recrystallized, depending on the composition of the steel and if the final rolling pass is scheduled to occur prior to quenching (Kömi et al., 2016). According to Chen et al. (2014), a fine texture dual-phase microstructure or complex martensite-bainite microstructure is expected for these types of steels, which is also confirmed by microstructural analysis in this study. The chemical composition of the material under investigation, based on the manufacturer's specifications, is presented in Table 2.1.

Table 2.1: The chemical composition limits (wt %)

C	Si	Mn	P	S	Al	Nb	V	Ti	Cu	Cr	Ni	Mo	N	B
0.097	0.2	1.09	0.008	0.001	0.034	0.001	0.009	0.02	0.033	1.13	0.38	0.191	0.005	0.0015

Microstructure analysis was carried out by means of optical microscopy, X-ray diffraction and scanning electron microscope (SEM). According to these measurements, the microstructure of S960 MC is a mixture of lath martensite (as a metastable solid solution phase) and bainite (as a mixture of carbide particles and ferrite), accompanied by scattered self-tempered martensite.

The prior-austenite grain size of the base material was measured on a sample after 5 minutes of etching in picric acid (1.5 g of picric acid + 100 ml of ethyl alcohol + 1 ml sodium alkyl sulfonate ["Agepol"] + 4–6 drops of HCl) at room temperature. The average size of prior-austenite grain was calculated (based on sum of the line lengths divided by sum of the grain boundary intersections) as about 60.9 µm, 11 µm and 50.6 µm in a rolling direction, transverse direction and normal direction respectively, yielding the value of 32.4 µm as total average size. The information provided by these measurements was utilized in the numerical modelling of a S960 MC notched specimen, which is discussed in Chapter 5.

2.2 Uniaxial tensile tests

Two identical tensile tests were performed on standard round specimens, according to ASTM (American Society for Testing and Materials) Standard E8M (2011), at the strain rate of 10^{-1} 1/s and with a gauge length of 30 mm. The monotonic tensile properties of the material are given in Table 2.2.

Table 2.2: The monotonic properties of S960 MC

$\sigma_{y0.2\%}$ (MPa)	σ_u (MPa)	E (GPa)	K (MPa)	n	σ_f* (MPa)	ε_f**	RA (%)
1040	1240	197	1440	0.0325	1945	1.11	67

* Corrected by the Bridgman correction factor
** Determined from the minimum cross-section diameter

2.3 Low-cycle fatigue tests

A systematic study was performed first on 25 samples, laser-cut form the main plate, in order to find the optimum machining parameters (feeding rate, cutting depth and speed) producing the least surface residual stresses after machining. Cutting fluid was used during the whole machining process. Therefore, these optimum parameters were used in order to make the final fifteen round specimens as follows:

- The first layers of the specimens were coarse machined (feeding rate = 0.2 mm/rev, cutting depth = 0.2 mm, cutting speed = 50 m/min)
- The final dimensions and surface were produced with fine machining (feeding rate = 0.1mm/rev, cutting depth = 0.1 mm, cutting speed = 70 m/min)
- Specimens were electro-polished at the end to acquire the desired configuration.

Specimens were made in such a way as to produce the final samples longitudinally, in the rolling direction of manufacturing process, so that the applied remote loading during tests runs parallel to this direction. The procedure for the specimens' preparation, including surface roughness and residual stress measurements, is reported in P-I. A servo-hydraulic material testing machine was used to conduct the experiments at room temperature. The load train was aligned by using a straight bar with four strain gages circumferentially attached to its surface.

Tests were conducted under the fully reversed strain-controlled mode in the form of a strain-versus-time triangular waveform, in accordance with the ASTM Standard E606 (2013). Five different strain amplitudes, ranging from 0.5 to 1.2%, were used and three specimens were tested at each amplitude. The failure criterion was defined as 50% load drop, as recommended by ASTM Standard E606. The applied loading frequencies started from 0.15 Hz and increased as the strain amplitude decreased in such a way that the strain rate was kept constant at all amplitudes.

In addition to plain specimens, eight round specimens were prepared and circumferential semi-circular notches with a radius of 0.5 mm and 1.5 mm were introduced to the specimens. Two load cases were used in the experiments. The maximum load was selected to keep the net stress less than the value of general yielding (less than 0.8 σ'_y , cyclic yield strength). Tests were conducted in the fully reversed (zero mean stress) load-controlled mode until the total rupture of the specimens. The experimental values of applied loads and total cycles to failure are shown in Table 2.3.

Table 2.3: Load cases, nominal applied values and total cycles to failure

Load case	Specimen's ID	Notch radius (mm)	Target force amplitude (kN)	Cycles to failure
1	N1	1.5	11	19,042
	N8			29,718
	N3	0.5	21	8,715
	N4			9,440
2	N5	1.5	10	41,402
	N6			47,923
	N9	0.5	20	26,698
	N11			29,750

2.4 Fracture surface study

The fracture surfaces of the tested specimens were analyzed to define their fracture mechanism. Two unnotched specimens (SP02 and SP35 with a strain amplitude of 0.5% and 1.2% respectively) and two notched specimens (N1 and N3) were investigated. Dry air blasting was used for fracture surface cleaning prior to fractography, as recommended by Zipp & Dahlberg (1987), as this is the least aggressive cleaning technique for removing lint and lightly adhered materials. The fracture surface of plain specimens showed the typical fatigue fracture posture, with its appearance getting rougher from the crack initiation site, the crack growth region, to the overload area and final fast fracture zone. SEM images of fatigue fracture surfaces, along with their full description, can be found in P-V.

SEM macrographs of the two notched specimens are presented in Figure 2.1. Fatigue crack and fast fracture overload regions are separated with black dashed lines. No significant difference can be seen between the ratio of rough and smooth fracture surface zones of N1 and N3. Regardless of the degree of stress concentration, the fracture surfaces of the notched samples consisted of fatigue crack growth area and dimples (micro-void coalesce) in the fast fracture zone. The existence of elongated dimples is a sign of shear as an active failure mechanism in the final overload area. SEM images showing the secondary particles as nucleation sites at the root bottom of the dimples can be found in P-V.

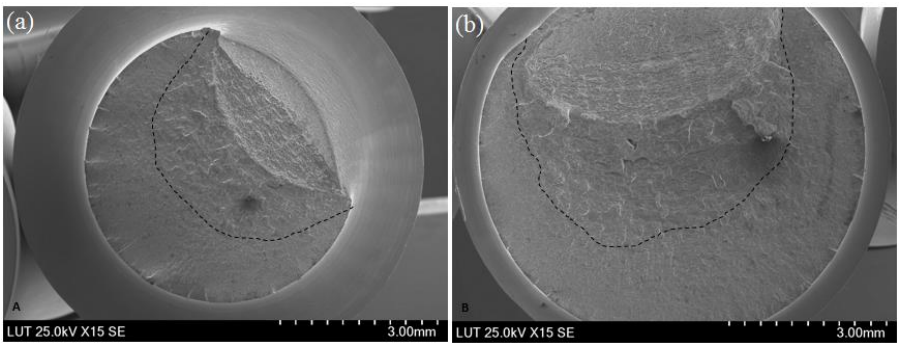

Figure 2.1: SEM macrographs of (a) N1 (high load, a low SCF), (b) N3 (high load, a high SCF)

3 The low-cycle fatigue analysis of plain specimens

The results of the fatigue tests based on strain amplitudes and total lives are given in Appendix I. The cycles at half of the lives were considered as exhibiting stabilized behaviour. The stresses and strains were defined at this stage to obtain the cyclic parameters of the material (n' and K', which are the cyclic strain hardening exponent and cyclic strength coefficient respectively). The test data at different strain amplitudes and the total fitted curve are shown in Figure 3.1.

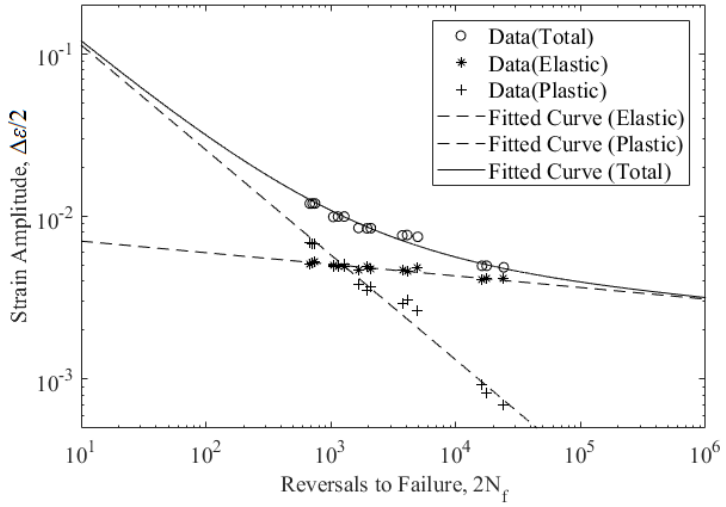

Figure 3.1: The strain-life curve of S960 MC

The fatigue properties and transition life (N_t) of S960 MC are listed in Table 3.1.

Table 3.1: Cyclic and fatigue parameters of S960 MC

Parameters	$\sigma'_{y\,0.2\%}$ (MPa)	K' (MPa)	n'	σ'_f (MPa)	b	ε'_f	c	N_t (cycles)
Values	833	1400	0.0835	1636	-0.07	0.5	-0.64	630

3.1 The numerical simulation of stabilized cyclic response

The cyclic stabilized response of S960 MC was simulated by means of the FE method. Strain rate–independent material properties were applied, along with the von Mises yield criterion.

3.1.1 Calibration

A model equipped with a combined non-linear kinematic-isotropic hardening rule (Lemaitre & Chaboche, 1990) was used. The results of fatigue tests at a given strain amplitude were selected and tabular data of different cycles running up to stabilization

were used as pair values of equivalent stress (σ_i^0) and equivalent plastic strain ($\bar{\varepsilon}^{pl}$) in order to define the isotropic hardening component of the model:

$$\sigma_i^0 = \sigma_i^t - \mu_i, \tag{3.1}$$

$$\bar{\varepsilon}_i^{pl} = \frac{1}{2}(4i-3)\Delta\varepsilon^{pl}, \tag{3.2}$$

where μ is the mean stress value of compressive and tensile stresses at each cycle, denoted by i. The kinematic hardening parameter was defined using the full hysteresis loop at stabilization and a model with one back stress tensor is used, which defines the translational centre of the yield surface in the stress space. The detail of the calibration process, along with utilized data from experimental hysteresis and stabilized loops at different strain ranges, can be found in P-1.

A comparison of the experimental and simulated stabilized hysteresis loops at ε_a = 1% for SP27 is shown in Figure 3.2. It can be seen that the model is capable of catching the overall shape of the hysteresis loop at the top and bottom tip points and it accurately shows the same value of plastic deformation. A slight discrepancy, however, can be seen in the ascending and descending trends, which may stem from the calibration process, because of the error introduced by noise filtering.

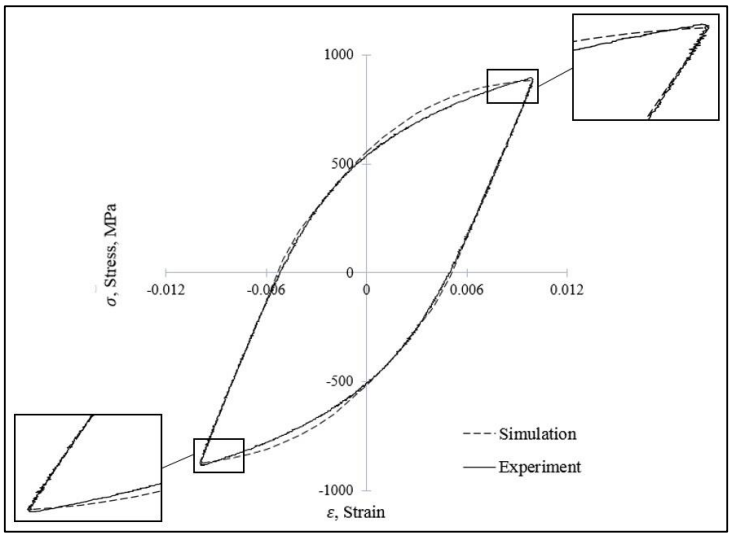

Figure 3.2: A comparison of the stabilized hysteresis loop from the experiments and the FE model for SP27 at cycle 320

3.2 Approaches for strain-life fatigue curve estimation

Knowledge of the fatigue properties of materials is essential for fatigue analysis and such information can be obtained by conducting fatigue tests. In this section a few

approaches and techniques are reviewed and investigated which provide an easier method for estimating the strain-life fatigue curve under the uniaxial loading condition. In this way, the costly and time-consuming fatigue tests can be prevented, in addition to providing a reliable and easy-to-use method for practitioners and design engineers. The available methods for the estimation of strain-life fatigue curves are divided into three categories: simple approximations, models based on continuum damage mechanics (CDM) and the proposed model based on ANNs (which is explained in detail in Section 3.2.3). The strain-life curve estimation capability of the selected methods is then investigated by their application to S960 MC.

3.2.1 Simple approximations

There are a few estimation methods that are able to estimate the strain-life curve just by using the monotonic material properties. The best-known approaches are those by Manson (1965), Mitchell et al. (1977), Muralidharan & Manson (1988), Bäumel et al. (1990), Ong (1993), Roessle & Fatemi (2000), Meggiolaro & Castro (2004) and the modified Mitchell method (Park & Song, 2003), proposed exclusively for aluminium and titanium alloys. No in-depth review of the aforementioned approaches is presented here and only the most promising estimations are chosen for investigation. The interested reader is referred to P-II and articles by Park & Song (1995) and Lee & Song (2006) for detailed reviews.

Three approximations are selected to be investigated and are applied to the material in question, namely those by Muralidharan & Manson (1988), based on the modified method of universal slopes (Equation 3.3); by Roessle & Fatemi (2000), based on hardness values (Equation 3.4); and by Meggiolaro & Castro (2004), based on constant parameters (Table 3.2).

The following equation is the approximation by Muralidharan and Manson:

$$\frac{\Delta\varepsilon}{2} = 0.623\left(\frac{\sigma_u}{E}\right)^{0.832}(2N_f)^{-0.09} + 0.0196(\varepsilon_f)^{0.155}\left(\frac{\sigma_u}{E}\right)^{-0.53}(2N_f)^{-0.56}, \tag{3.3}$$

where σ_u and ε_f denote ultimate tensile strength and true fracture strain respectively, and E stands for Young's modulus.

The following is the approximation by Roessle and Fatemi:

$$\frac{\Delta\varepsilon}{2} = \frac{4.25(HB)+225}{E}(2N_f)^{-0.09} + \frac{0.32(HB)^2 - 487(HB)+191000}{E}(2N_f)^{-0.56}, \tag{3.4}$$

where HB is the Brinell hardness and E is the modulus of elasticity in MPa.

The following is the approximation by Meggiolaro and Castro:

Table 3.2: Proposed values by Meggiolaro and Castro for fatigue properties of steels

Properties	Values
Fatigue strength coefficient, σ'_f(MPa)	1.5×σ_u
Fatigue strength exponent, b	-0.09
Fatigue ductility coefficient, ε'_f	0.45
Fatigue ductility exponent, c	-0.59

In a statistical evaluation of methods, Meggiolaro and Castro concluded that using exclusive median values for the fatigue properties of different groups of materials (steels and aluminium alloys) yields the closest predictions to experimental values. They questioned the correlation of the fatigue coefficients, especially ε'_f, with any monotonic measure of material ductility and proposed constant values for this property and both fatigue exponents. Roessle & Fatemi (2000) also showed that the assumption of ε'_f being related to true fracture strain ε_f is not valid as there is no correlation between these two parameters, and usage of relations to correlate these two parameters could lead to significant error. These findings led to the proposal of constant values for both fatigue exponents and the fatigue ductility coefficient. Only the fatigue strength coefficient is related to the materials ultimate tensile strength. The validity of the three proposed approximations, which are the most recent and most promising methods for simple estimation of the strain-life curve of different groups of materials, is examined and shown in Figure 3.3.

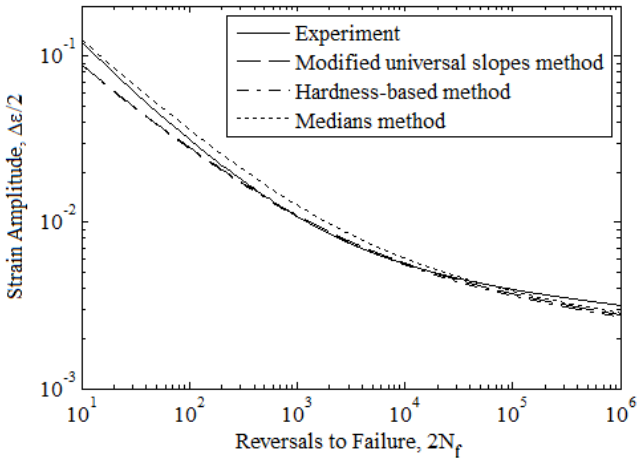

Figure 3.3: A comparison of estimated curves by simple approximations with the curve of the experiment

3.2.2 Approximations based on continuum damage mechanics

The current study uses a method proposed by Bhattacharya & Ellingwood (1999) using basic principles of mechanics and thermodynamics, as it requires a minimal number of

mechanical properties to tune the model for the estimation of the fatigue life curve in the low-cycle regime. P-II provides the reference to other models based on CDM and clarification of the selected model. Using a constitutive law, based on the Ramberg–Osgood relationship applied to the effective stress–strain relation, an isotropic damage growth model under uniaxial monotonic loading was developed by Bhattacharya & Ellingwood (1999). This model relates the damage initiation to the accumulation of threshold strain (ε_0) and considers the plastic strain (ε_p) as the main factor for damage growth:

$$D = 1 - \frac{C_2}{\varepsilon_p^{(1+n)} + C_1}, \tag{3.5}$$

where C_1 and C_2 are parameters determined by using the material's hardening exponent (n), coefficient (K), true fracture strength (σ_f) and threshold strain (ε_0). Plastic strain equal to this threshold value corresponds to zero damage and plastic strain equal to true fracture strain (ε_f) corresponds to critical damage (D_c). This model hypothesizes that damage will increase by reloading the section above the endurance limit, S_e, which can be approximated as S_e = 0.7×(0.5σ_u) (Bennantine et al., 1990). In the case of strain-controlled loading, the relationship to express the progress of the damage (D_N) with the number of cycles (N) defined as:

$$D_N = 1 - (1 - D_0)\left[\frac{\frac{1}{1+n'}\Delta\varepsilon_{p0}^{(1+n')} - \Delta\varepsilon_{p1}^{n'}\Delta\varepsilon_{p0} + C}{\frac{1}{1+n'}\Delta\varepsilon_{p}^{(1+n')} - \Delta\varepsilon_{p1}^{n'}\Delta\varepsilon_{p} + C}\right]^N. \tag{3.6}$$

For a virgin material, the initial damage (D_0) is zero. The cyclic strain hardening exponent is defined by n' and $\Delta\varepsilon$ defines the strain range. The strain ranges $\Delta\varepsilon_0$ and $\Delta\varepsilon_1$ correspond to the endurance limit and zero stress on the ascending part of the stress-strain coordinate respectively, and the subscripted p indicates the plastic component of the strain ranges. The former is defined in the Ramberg–Osgood equation form, using only the plastic part. Parameter C can be described as:

$$C = \frac{3}{4}\frac{\sigma_f}{2^{(1-n')}K'} - \frac{1}{1+n'}\Delta\varepsilon_0^{(1+n')} + \Delta\varepsilon_{p1}^{n'}\Delta\varepsilon_0, \tag{3.7}$$

where K' stands for the cyclic strength coefficient. Upadhyaya & Sridhara (2012) stated that a critical damage value calculated using monotonic properties is an applicable criterion for fatigue cyclic loading. Therefore, using Equation 3.5 along with the monotonic data from Table 2.2, the critical damage D_c corresponding to $\varepsilon_p = \varepsilon_f$ was obtained as 0.51, which is in the range of 0.15–0.85, the range reported as typical of experimental data by Lemaitre (1992). Definition of the critical damage value and the cyclic and monotonic material behaviour enables the model to predict the crack initiation life of the material under investigation. Values from Tables 2.2 and 3.1 were used with Equations 3.6 and 3.7 and the predicted curve is shown in Figure 3.4.

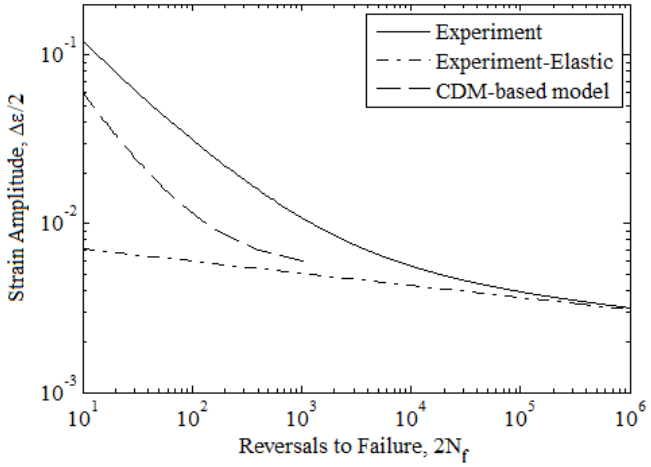

Figure 3.4: A comparison of the estimated curve of the CDM-based model with the curve of the experiment

3.2.3 **Approximations based on artificial neural networks**

The last category of methods applied to strain-life curve estimation is a model based on ANNs. The mathematical detail supporting this technique can be found in detail in a publication by Schalkoff (1997). This technique, working analogously to biological neural networks, has demonstrated considerable potential in the modelling and simulation of correlations – both linear correlations and the highly non-linear relationships that are difficult to describe with physical models. The technique has proven its potential in the fatigue life prediction of different types of steels under different fatigue life domains, ranging from low- to high-cycle fatigue and even under creep-fatigue interaction conditions (Pujol & Pinto, 2011; Pleune & Chopra, 2000; Srinivasan, 2003). Due to the lack of studies assessing the ability of ANN approaches to provide fatigue data from monotonic properties, the current study scrutinizes this approach in terms of its usability compared to other methods.

In the area of strain-life estimation, Genel (2004), using five monotonic properties (the modulus of elasticity, reduction in area (RA), hardness, yield strength and ultimate tensile strength) of 73 steels (carbon and alloy steels), developed an ANN-based model that was able to estimate the fatigue properties separately with an extremely high level of accuracy (the correlation coefficients were greater than 99% for all parameters). However, studies have strongly indicated a lack of correlation between monotonic properties and most fatigue properties (Meggiolaro & Castro, 2004; Basan et al., 2010; Basan et al., 2011), which is also examined and verified in the current study for 60 low-alloy steels (listed in Appendix II) [data from MATDAT (Basan, 2017)]. The lack of an evident correlation between most fatigue properties and monotonic properties is the main reason for the use of constant values for the fatigue properties ε'_f, b and c of steels

and aluminum alloys by Meggiolaro & Castro (2004) and most other approximation methods.

Given the uncertainty surrounding the existence of a correlation, the use of the type of ANN model proposed by Genel for the estimation of individual fatigue properties from monotonic properties seems problematic and the model is thus not used in this study. Therefore, a new ANN-based model is developed for the estimation of the strain-life curve. This model takes all four fatigue properties into account in the process of strain-life curve estimation [utilizing the method of Basan et al. (2011)], but unlike Genel (2004), they are lumped together, that is, the correlation is established between the monotonic properties and reversals to failure rather than by each parameter individually.

Investigating data from 32 normalized steels, and quenched and tempered low-alloy high-strength steels, Basan et al. (2010) only found a clear correlation between hardness and the fatigue strength coefficient. The same trend was also observed for unalloyed and high-alloy steels and for aluminium and titanium alloys (Basan et al., 2011). This finding implies that constant values should be used for the other three fatigue parameters (b, c and ε'_f) for these materials. In addition, the strong correlation shown between hardness, ultimate tensile strength and yield strength in steels (Pavlina & Van Tyne, 2008) suggests that the correlation will also be valid between the fatigue strength coefficient and these two strengths. Basan et al. (2010) proposed a method that relates the hardness to the logarithm of the experimental number of reversals to failure (defined as crack initiation life in the strain-life approach) at different strain ranges and obtained their correlation. In this study, the validity of this assumption was also checked for the current data set. It can be seen from Figure 3.5 that a correlation exists between hardness and the reversals to failure estimated by experimentally obtained fatigue properties. The gradient of the trend depends on the strain range and the corresponding number of reversals compared to the transition fatigue life.

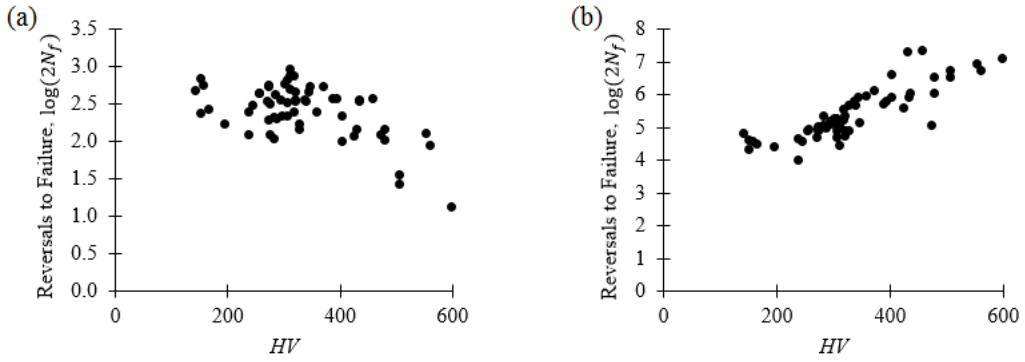

Figure 3.5: A logarithm of the number of reversals to failure versus hardness when (a) $\Delta\varepsilon/2$ = 2% and (b) $\Delta\varepsilon/2$ = 0.3% for the 60 low-alloy steels used as a data set for network implementation

Therefore, the hypothesis of the correlation between monotonic properties and the number of reversals to failure was utilized in this study and combined with an ANN-based model for strain-life curve estimation. The steps required for the implementation of the networks – such as data collection, network establishment, configuration and initialization – are explained in detail in P-II. The results of life estimations by the ANN-based model for five strain ranges are used in the current study. The strain-life estimation by the ANN-based model is shown in Figure 3.6.

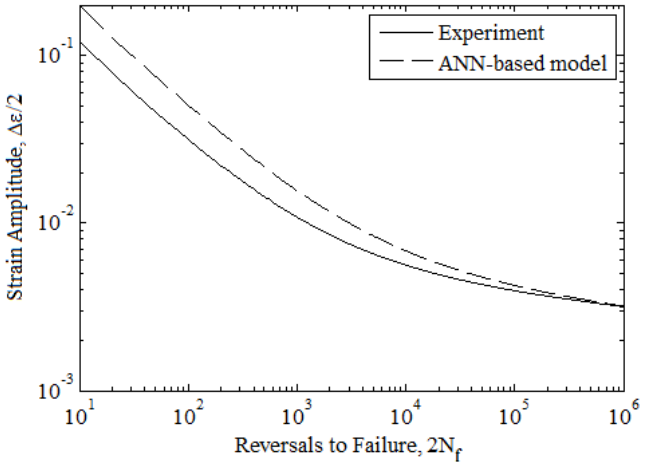

Figure 3.6: A comparison of the experimental strain-life curve of S960 MC with the estimated curve created by the ANN-based model

3.3 Discussion on the accuracy of the investigated methods

The method based on the modified universal slopes was selected as the best representative of the category of simple approximations, based on the strain amplitude variation diagram, for the material under investigation. Lee & Song (2006) also found that this method provides the best estimation for low-alloy steels and stated that it should be used as the first choice method in the fatigue analysis of this group of steels.

In the category of CDM-based models, only the method proposed by Bhattacharya & Ellingwood (1999) was chosen because of its simplicity. Other CDM-based models were not investigated as either their validity for the LCF condition is unconfirmed or they require detailed experimental data, making them unsuitable for use by practitioners. The predicted curve using the CDM-based model tends toward the elastic line of the experimental curve as the number of cycles increases. The same trend was also seen in the original study for two other types of steels (Bhattacharya & Ellingwood, 1998). The theory used for the development of this model as an approach for prediction of the early stages of the crack initiation phase (smaller cracks in size compared to those in the conventional strain-life approach) could explain the higher conservatism of the predicted curve compared to the experimental curve and the other estimated curves.

The curve estimated by the ANN-based model also gives acceptable results at a medium to high number of cycles to failure, with its maximum accuracy for reversals higher than 10^5. Although no mechanical theory supports the application of the ANN method in estimation of the strain-life curve, and subsequently fatigue properties, the results show the potential of this technique to act as an approximation method. It should be mentioned that the current model is implemented mainly on the concept of correlation between monotonic properties and fatigue life proposed by Basan et al. (2010). Therefore, besides the inherent limitations of the ANN technique for this specific application, uncertainties in the concept itself could act as a source of error in the estimations.

Although non-linear curve fitting (in the form of the Coffin–Manson relationship) could give the fatigue properties, it should be highlighted that these values are not unique, as different networks – even with high levels of correlation in regressions – could yield slightly different life estimations. Therefore, in order to mitigate this variation and obtain more stable estimations for fatigue coefficients, the constant values for fatigue exponents were considered as b = -0.08 and c = -0.63, which were selected as the mean values for all the low-alloy steels used as the data set. These values differ from the constants that are considered by the modified universal slopes and hardness-based methods for steels. Based on the data set comprising of 60 low-alloy steels, the constant values considered in the current study better define the fatigue exponent values of low-alloy steels, which is also confirmed by the experimentally gained values for S960 MC. Curve fitting by non-linear regression through estimated lives by using the ANN-based model, along with the consideration of constant values for the fatigue exponents, yielded estimations of σ'_f = 1822 MPa and ε'_f = 0.8 for S960 MC.

Of all three categories of methods studied here, it can be concluded that the method based on modified universal slopes, requiring only simple monotonic properties, gave the best estimation of the strain-life curve when compared with the experimental curve of the material under investigation.

4 Extending the ANN-based models to the estimation of the stress concentration factor of welds

Welding is the most common joining process used in the fabrication of components and structures. Although the high strength steels, benefiting from their strength–weight ratio, are used in very demanding engineering applications, the welded components of these materials could suffer from losing their strength due to the flaws, high residual stresses and other imperfections introduced to the component by improper welding (microstructurally and geometrically). Because of being exposed to in-service cyclic loads, these welded parts are susceptible to fatigue failure and their analysis is an inevitable part of the design process. The term *stress concentration* and the factor defining it (the SCF), form one of the main parameters which is estimated and used in the fatigue analysis of notched components, such as welded joints. This factor can be obtained experimentally, analytically and numerically; among them the numerical methods, such as the FE method, can be considered the most accurate.

As confirmed by the investigations in the previous chapter, the ANN-based models can be used successfully in order to define the relations (linear to highly non-linear) between related parameters. In this section, it is tried to utilize this technique in the estimation of SCF in welds. Knowing the fact that the implementation of a successful network strongly depends on its input data, special attention was paid to defining the effective profiles (by using an appropriately designed experimental method) and their modelling using the FE method.

4.1 The investigated configurations

In a successful attempt, the application of ANNs was extended to the calculation of the SCFs of different weld types, such as T-welded and butt-welded joints, schematically shown in Figures 4.1 and 4.2 respectively.

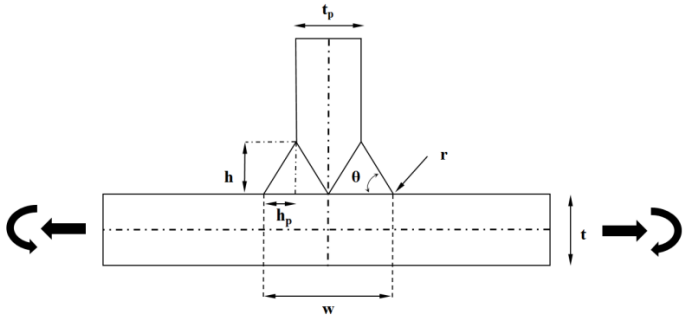

Figure 4.1: The configuration of a T-welded joint and effective parameters for the SCF

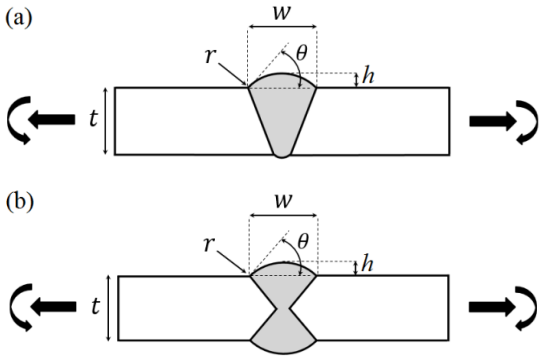

Figure 4.2: The configuration of a (a) single-V butt weld and (b) double-V butt weld

First of all, a literature review was performed in order to obtain the common empirical equations used for SCF calculation for these welded joints in order to define and select the best and most accurate proposal for comparison. This led to the selection of both the empirical equations proposed by Brennan and Helier (Brennan et al., 2000; Hellier et al., 2014) for T-welded joints and that proposed by Kiyak et al. (2016) for butt-welded joints. Only these equations are listed below and different proposed equations are left out of this section. The reader, however, is referred to P-III and P-IV for an in-depth review of these equations.

The equation used as the reference for comparison is the one proposed by Brennan et al. (2000) for SCF calculation for T-welded joints in as-welded condition both under an axial load (theta in radian):

$$SCF_a = 1.1 + 0.067\theta - 0.25(r/t) - 0.04(w/t) + 0.003\theta^2 - 12(r/t)^2 - 0.014(w/t)^2 + 0.0164\theta^3 - 0.0005(w/t)^3 + 0.00004(w/t)^4 - 0.3\theta(r/t) - 0.023\theta(w/t) + 0.91(r/t)(w/t) - 8.3\theta^2(r/t) + 0.225\theta^2(w/t) + 100.5\theta(r/t)^2 - 0.0792\theta(w/t)^2 - 37.5(r/t)^2(w/t) + 0.908(r/t)(w/t)^2 + 0.27\theta^{0.19}(r/t)^{-0.47}(w/t)^{0.25}, \quad (4.1)$$

and under a bending load:

$$SCF_b = 1.14 + 0.13\theta - 0.67(r/t) - 0.083(w/t) + 0.08\theta^2 + 28(r/t)^2 - 0.02(w/t)^2 + 0.01\theta^3 - 0.0005(w/t)^3 + 0.00002(w/t)^4 - 4.3\theta(r/t) - 0.09\theta(w/t) + 1.03(r/t)(w/t) - 13.7\theta^2(r/t) + 0.443\theta^2(w/t) + 150\theta(r/t)^2 - 0.13\theta(w/t)^2 - 62(r/t)^2(w/t) + 1.53(r/t)(w/t)^2 + 0.005\theta^3(w/t) - 30\theta(r/t)^3 + 3.57\theta(r/t)(w/t) + 5\theta(r/t)^2(w/t) + 0.35\theta^{0.26}(r/t)^{-0.468}(w/t)^{0.3}. \quad (4.2)$$

The investigation continued by scrutinizing the ability of ANN-based models to be used in the SCF calculation of butt-welded joints. This joint type was studied under axial and bending loads in both single-V and double-V forms. Based on the literature review, the

most recent and accurate empirical equation proposed by Kiyak et al. (2016) was chosen for a comparison of the results:

$$K_t = 1 + p_1.\left(\frac{h}{t}\right)^{p_2.\theta}.\theta^{p_3}.e^{-p_4.\theta}.\left(\frac{r}{t}\right)^{-0.295.\theta}.(0.021 + \frac{r}{t})^{-p_5}. \quad (4.3)$$

Table 4.1: The coefficients in Equation 4.3

Type of butt weld	p_1	p_2	p_3	p_4	p_5
Single-V (axial tension)	1.3905	0.2081	1.0756	1.7483	0.4413
Single-V (bending)	1.5326	0.2857	1.1036	1.5436	0.4287
Double-V (axial tension)	1.9220	0.3224	1.1257	1.5481	0.4002
Double-V (bending)	1.1399	0.2062	1.0670	1.6775	0.4711

4.2 Design of the experiments

Taguchi methods were used in order to perform the design of experiments and to obtain the optimal number of configurations and their local weld parameters for both the T-welded and butt-welded joints that were to be modelled by the FE method. In Taguchi methods, experimental results are analysed with the following aims:

- To establish the optimal or best possible condition for launching a process or a product
- To evaluate the effect of each factor separately
- To assess the response under optimized conditions.

This design method attempts to recognize the controllable factors that are involved in the minimization of the effect of uncontrollable parameters (noise parameters). In the case of T-welded and butt-welded joints in the current study, the design of experiments led to a few hundred profiles – their design parameters and levels are reported in P-III and P-IV.

4.3 Finite element modelling

All the configurations were postulated as fully penetrated joints and exposed to axial tension and bending loads (and combined axial-bending in the case of T-welded joints). In the case of butt-welded joints with misalignment, only the membrane load was considered to specifically investigate the secondary bending effect imposed on the joint due this axial eccentricity. Distinct networks were trained, validated and tested for each configuration. A mesh convergence study was performed according to the recommendation of Fricke (2012) in order to obtain the optimum mesh size and number. P-III and P-IV can be consulted in order to obtain detailed information regarding the numerical modelling and considered weld profile parameters.

4.4 Results and discussion

A comparison of the results of the most accurate empirical equation for T-welded joints (in the absence of undercut) and the ANN-based model is shown in Figure 4.3. The comparison is done for both axial and bending loads.

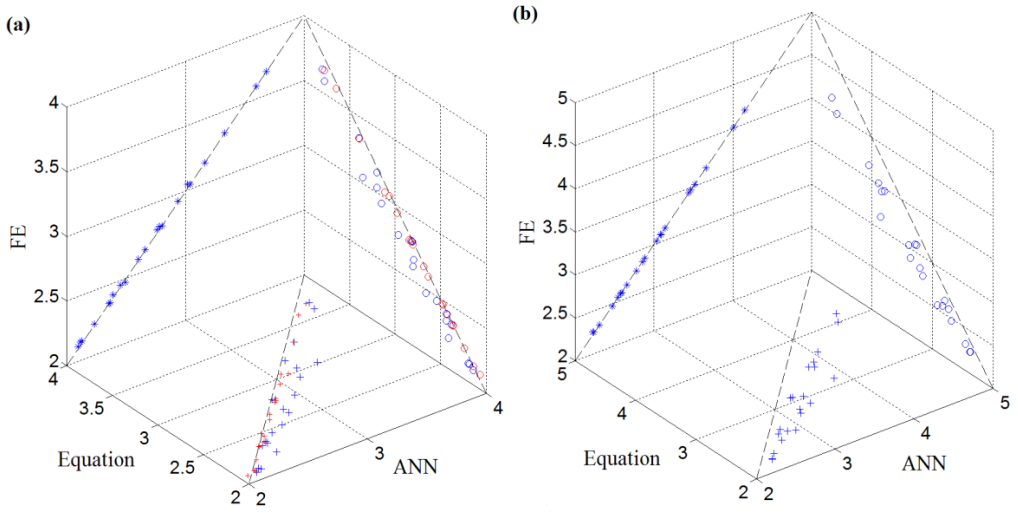

Figure 4.3: A comparison of the calculated SCFs using the empirical equations (4.1 for a and 4.2 for b), the ANN-based model and FE model for (a) axial and (b) bending loads

It can be seen from Figure 4.3 that the estimations of the ANN-based model have a much higher correlation degree with the FE model. In T-welded joints, in addition to the local weld parameters, the effect of undercuts (either as a weld defect or a consequence of post-weld treatment) was studied and numerical models explicitly considering this parameter were simulated. No empirical equation is available capable of taking this parameter into account in the calculation of SCFs.

There are red marks in Figure 4.3a which are the estimations made by the modified version of the original equation proposed by the same authors (Hellier et al., 2014) for axial loading:

$$SCF_a(modified) = 0.889 - 0.302\theta + 3.44(r/t) + 0.529(w/t) + 0.012\theta^2 + 104(r/t)^2 - 0.633(w/t)^2 - 0.614\theta^3 + 0.18(w/t)^3 - 0.018(w/t)^4 - 35.5\theta(r/t) - 0.153\theta(w/t) + 4.38(r/t)(w/t) + 30.6\theta^2(r/t) - 0.219\theta^2(w/t) - 64.3\theta(r/t)^2 + 0.041\theta(w/t)^2 - 54.5(r/t)^2(w/t) + 0.595(r/t)(w/t)^2 + \theta^{0.68}(r/t)^{-0.299}(w/t)^{0.263}. \quad (4.4)$$

Although the modified equation yields much higher accuracy in SCF estimation, its degree of derivation from FE results is still slightly more than those derived from ANNs. In addition to providing a method with higher accuracy, the ANN-based model

was coupled with a genetic algorithm in order to provide the best set of local weld parameters, resulting in the least SCFs. A detailed description of the implemented network, along with its analysis of errors, can be found in P-III.

Similar to the models of T-welded joints, the ANN-based models showed a high level of accuracy in the calculation of SCFs of butt welds when compared with the empirical equation. In addition, a specific network was implemented in order to be able to explicitly consider the axial misalignment effect on the SCFs of butt welds. The modelling technique, network structure and implementation, analysis of variance and comparison of results with those joints studied using the common empirical equations for misalignment analysis are provided in P-IV.

Figure 4.4 shows the results of SCF calculations by the ANN-based model and Equation 4.3 when compared with those of the FE model. It can be seen that the trained networks were able to estimate the SCF values with a considerably higher degree of precision (the coefficients of determination were greater than 99.9% in all load cases and configurations). Equation 4.4, however, did not yield equally accurate estimations and this discrepancy increased in joints with higher SCF values. A possible explanation for this discrepancy compared to FE model results and its absence in the original study (Kiyak et al., 2016) could be the utilization of remote nominal stress in the calculation of SCFs instead of the linearized through-thickness stress utilized in the current study. The evaluation of errors in SCF estimations showed that using the nominal stress instead of linearized through-thickness stress yields an error in the same range as reported in study of Kiyak et al. (2016) (ranging from ≤3.5% to ≤4.4%, depending on the configuration and load type). It should also be highlighted that only profiles in which the local weld parameters were within the valid range of the proposed equation were selected for comparison with FE results.

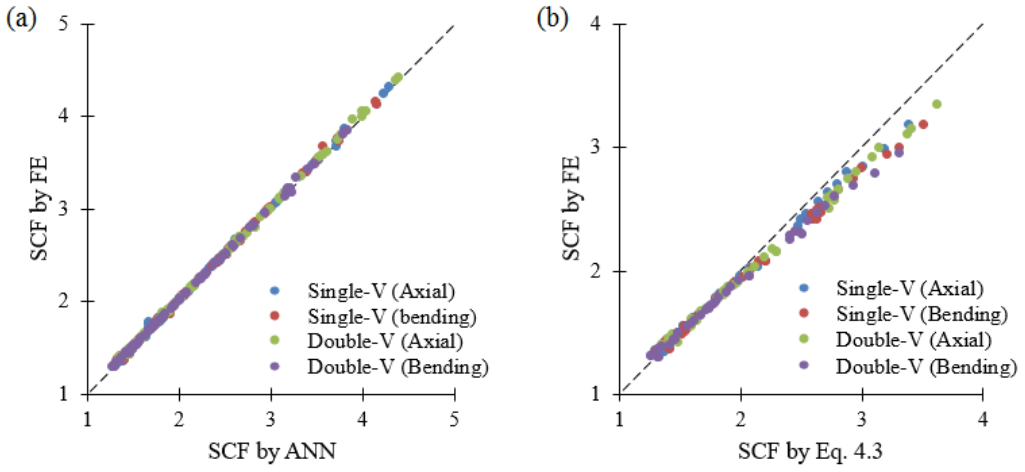

Figure 4.4: A comparison of estimated SCF values by (a) the ANN-based model and (b) Equation 4.3 with FE model results

A comparison with the conventional method of using a stress magnification factor to modify the nominal stress and distinct values of SCFs for membrane and bending stress components of axially-misaligned joints was also performed to illustrate the accuracy of the ANN-based model in the estimation of SCFs for a butt-welded joint with axial misalignment. The results also showed improvements in the calculations for this type of joint. A full comparison can be found in P-IV.

5 The low-cycle fatigue analysis of notches

Some well-known methods for conventional notch fatigue analysis, mainly based on the philosophy of critical distances, are the proposals by Peterson (1959) and Neuber (1958). Although entirely empirical and without any physical support, these proposed methods still provide fairly acceptable estimations, mainly under uniaxial loading conditions, and different modifications are also proposed to improve its estimation accuracy, for example modifications of Neuber's rule (Kujawski & Sree, 2014; Zappalorto & Kujawski, 2015). There are, however, numerous investigations in the literature, such as those by Buch (1984) and Ciavarella & Meneghetti (2004), questioning the viability of these simple single-parameter approaches and their ability to deal with notch size effects arising from deformation and damage phenomena. For instance, it was pointed out by Ciavarella and Meneghetti that the classical Peterson's relation is unable to analyse a notch with an infinitesimal root radius (a crack-like notch) because of the tendency of the fatigue notch factor towards unity. They also argued that the usability threshold of Neuber's rule is limited to notches sized a few tenths of a millimetre. Another approximation procedure that can be used in a manner similar to Neuber's rule is the strain energy density (SED) method, as described by Molski & Glinka (1981).

Local strain analysis at the notch root, based on the similitude concept and utilizing the numerical methods, is another technique suitable for notch analysis. However, its accuracy could be affected by the approach utilized by the user and by the geometrical features of the component. That is, this method is only able to predict accurate strain values at the notch root if detailed elastoplastic FE analysis using the cyclic material response is performed. Conducting the linear FE analysis equipped with approximations, such as Neuber's rule, in order to evaluate the strain could diminish its accuracy and lead to the incorrect estimation of critical spots in components, including stress raisers with different configurations (Taylor et al., 2000). This could happen because the linear models, coupled with empirical approximations, do not allow stress/strain distributions at the notch root because of plasticity. In addition, it has been shown (Fatemi et al., 2004) that the accuracy of this method can be affected by notch sharpness (i.e. the higher the SCF is, the more conservative the life estimations are).

5.1 The elastoplastic reformulation of the Theory of Critical Distances

In order to improve the notch sensitivity analysis and overcome the aforementioned difficulties (mostly related to correctly defining the fatigue notch factor) by consideration of the stress/strain gradient and notch root plasticity, a group of methods relying on the critical distances concept was developed (mainly by Taylor) under the name the theory of critical distances and showed promising results in both high and LCF analyses under uniaxial and multiaxial loading conditions (Taylor, 2007; Susmel & Taylor, 2003; Susmel, 2008; Gates & Fatemi, 2016). The elastoplastic modification of

the TCD approach (Susmel & Taylor, 2010), proposed for a LCF regime, states that, by directly post-processing the mechanical fields (i.e. elastoplastic stress–strain fields) at the notch root of a FE model, the detrimental effect of stress concentrators of any kind on the fatigue life can be taken into account. The versatility of this approach enables it to be applied in a variety of interpretations by simply changing the geometrical features and size of the domain in which the required effective strain is calculated. Two interpretations of the TCD in a LCF regime are namely the point method (PM) and line method (LM). In the simplest interpretation of the TCD approach, the PM, elastoplastic stress-strain values at a given point, distant from the notch root, are used in the estimation of fatigue damage. Under a LCF regime, this distance is postulated to be equal to a material characteristic length, depending only on the material, independent of notch geometry and load spectrums (Susmel & Taylor, 2010). The main advantage of such a technique is that the critical distance value no longer depends on the number of loading cycles to failure, as it happens instead when the TCD is applied by post-processing linear-elastic stress fields in high-cycle fatigue (Susmel & Taylor, 2007). This method, considering the characteristic length (L) in conjunction with the Coffin (1954), Manson (1954) and Smith-Watson-Topper (Smith et al., 1970) parameters can provide accurate life estimations under constant and variable amplitude loadings in both the presence and absence of mean stresses (Susmel & Taylor, 2010; Susmel & Taylor, 2015).

5.2 Coupling the crystal plasticity finite element method with the TCD

Being a successful technique that is able to provide improvements over conventional approaches, the TCD still is not supported by any physical backgrounds and does not explicitly consider the microstructure's heterogeneity. Although, it is postulated that the length parameter used in this approach might be related to microstructural units, such as grain size, this clear relation was only observed for the brittle fracture of steel under monotonic loading and no clear microstructural relationship is found in LCF and high-cycle fatigue applications (Taylor, 2006; Taylor, 2016).

An attempt was made to investigate the effect of introducing microstructural features on the estimation capabilities of this successful empirical approach. To this end, post-processing is performed on the results of a FE model equipped with the framework of constitutive equations based on crystal plasticity instead of the conventional FE model utilized in the TCD approach to represent the heterogeneity of the material's microstructure. The analysis covers two sections, starting with the cyclic plasticity analysis with polycrystals, utilizing a self-consistent scheme for model parameter identification. Both monotonic and cyclic tests are conducted in order to tune the constitutive equations' parameters, considering isotropic and kinematic effects. In the second section, a specimen with a circumferential round notch is simulated using the integrated material modelling technique. That is, the notch root is covered by the crystal plasticity zone and the rest of the model is analysed by a conventional continuum FE

formulation. This combined model is used in order to investigate the effect of microstructural heterogeneity along with size and gradient effects on the effective strain used in the reformulation of the TCD approach in LCF.

The total deformation framework suggested by Mandel (1973) was utilized for crystal plasticity modelling in the current study. Detailed information regarding the model can be found in P-V. In the following, a short description of the material parameters identification and numerical procedure used in the implementation of the CPFE model are provided.

5.2.1 The identification of material parameters

Modelling started with the identification of crustal plasticity parameters. The experimental data of Chapter 2 were used, along with the homogenization model proposed by Cailletaud & Pilvin (1994), known as the Beta-method, in order to transform the behaviour of single crystals into the homogenized behaviour of the polycrystalline microstructure. In the Beta-method, the elastoplastic tensor β is introduced to describe the interphase or intergranular constraints, or more precisely, the effect of other phases or grains. The module L can be chosen to be Kröner's approximation or simply equal to the shear modulus of the material. This can be written as:

$$\sigma^g = \Sigma + L^g : (\beta - \beta^g), \tag{5.1}$$

where σ and Σ are the stress tensors and the superscripted g denotes the term for a grain or phase. The evolution of tensor β can be written as:

$$\dot{\beta} = \dot{\varepsilon}_p^g - D^g \left(\dot{\varepsilon}_p^{g,Mises} \left(\beta^g - \delta^g \varepsilon_p^g \right) \right), \tag{5.2}$$

where D and δ are scale transition variables. A phenomenological hardening model that considers isotropic softening and kinematic hardening is used instead of a dislocation dynamics-based model, which means that hardening/softening is controlled by the accumulated plastic slip in the slip systems and their interactions. Table 5.1 shows the calibrated material parameters for the crystal plasticity model:

Table 5.1: Calibrated material parameters for the crystal plasticity model (All units in MPa)

Parameters	Elastic constants			Slip parameters							
	C_{11}	C_{12}	C_{44}	τ_0^{110}	τ_0^{112}	V	v	b_1	Q_1	b_2	Q_2
	219540	78125	70700	250	250	250	100	84	-9.5	8	-20

Interaction matrix coefficients	h_1	h_2	h_3	h_4	h_5	h_6	h_7	h_8
	1.3	1.0	1.05	1.15	1.1025	1.3	1.495	1.0

Kinematic parameters	q	d
	8500	250

5.2.2 The modelling procedure

An integrated modelling technique was used in the simulation of the notched specimen. That is, the notch root is encapsulated by a CPFE model, its covering zone by an elastoplastic conventional FE model, and the rest of the geometry by an elastic material model. The size of the CPFE zone must be as small as possible to minimize the computational time of three-dimensional model and at the same time broad enough to encapsulate the fatigue process zone. Although this zone is not necessarily the exact size of the plastic zone, a series of elastoplastic FE models were first checked, based on the accumulated equivalent plastic strain for up to 20 cycles, in order to make sure that the considered crystal plasticity zone is broad enough to fully cover this plastically deformed area. A cuboidal shape was utilized instead of realistic microstructure morphology. Due to the complex microstructural features of martensite, the element size was selected to be in the range of the measured prior-austenite grain size (25–35 μm). It is assumed that each grain comprises one packet of parallel martensitic laths, each with a random orientation.

5.3 Results and discussion

By post-processing the results of the conventional FE model and utilizing the TCD approach based on PM interpretation in its original form, the material characteristic length of L_{PM} = 149 μm away from the notch root was obtained. The life estimations obtained by using this length are depicted in Figure 5.1, showing great improvements, especially for specimens with a higher SCF compared with other common approximations. The level of unnecessary conservative fatigue life estimations was profoundly decreased in the specimens with sharper notches.

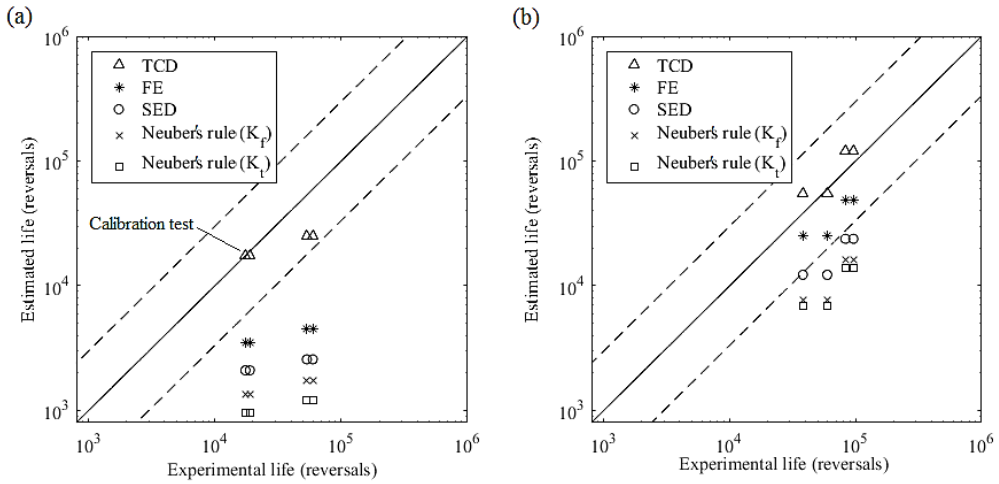

Figure 5.1: A comparison of fatigue life estimations by different methods for two notched specimens: (a) R = 0.5 mm (b) R = 1.5 mm (K_t and K_f denote using a SCF or fatigue notch factor in estimations)

The inhomogeneous distribution of mechanical fields in the critical area of the notch root makes it impossible to easily use the stress–strain gradient with the PM interpretation of the TCD. This issue can be sorted out by fitting a line (in linear or non-linear form) through the point distribution of strain values and using it as the strain curve for the estimation of the material characteristic length that is used in the TCD approach. This method is used by Musinski & McDowell (2012) in plotting the log-linear fit line through the point distribution of maximum fatigue indicator parameter (they use the Fatemi-Socie parameter in their study), obtained from a three-dimensional notched plate with crystal plasticity formulation at the notch root.

Thanks to having a three-dimensional model, it is possible to select the random paths in order to obtain the strain values at different locations. In the current study, five different paths were selected, denoted by P1 to P5. The estimated values of the material characteristic length obtained by linear and exponential fitting through the results from different random paths of the CPFE model (L_{PM}^{CP}) are listed in Table 5.2. The strain dispersal at the notch root around the model yields different strain gradients depending on the different paths selected around the notch root. However, it can be observed that the differences in the estimated values of L_{PM}^{CP} obtained from different paths are negligible and even identical for some paths. However, averaging these could provide a reference value with a higher degree of reliability in calculations. This, in a way, is comparable to the original form of the TCD proposed for LCF life estimations. Although using just one experimental result for calibration is satisfactory, in the case of having a high number of identical samples, it was proposed that the results of more than one experiment and the mean value of the material characteristic lengths should be used in fatigue life estimations (Susmel & Taylor, 2010).

Table 5.2: Estimated values of the material characteristic length

Parameter	Value (μm)	
	Linear fit	Exponential fit
L_{PM-P1}^{CP}	214	194
L_{PM-P2}^{CP}	192	180
L_{PM-P3}^{CP}	214	202
L_{PM-P4}^{CP}	214	197
L_{PM-P5}^{CP}	146	138
mean L_{PM}^{CP}	196	182
L_{PM}	149	

Figure 5.2a shows the estimated fatigue lives using the mean value of $L_{PM,}^{CP}$ approximated by both linearly and exponentially fitted lines through strain distribution. This is done as the L_{PM}^{CP} values from linear fitting showed more consistency in different paths, whereas the mean value from exponential fitting yielded a lower percent error compared with the L_{PM}. The differences are, however, negligible (especially for

notched specimens with a bigger notch radius) when it comes to the estimation of fatigue lives. Figure 5.2b shows the estimated fatigue lives, using material characteristic length that is approximated by both numerical models with and without the crystal plasticity zone and compared with the experiments. All estimations lie in the life boundary of factor ±3, which can be considered totally satisfactory considering the nature of the fatigue test results even on plain specimens.

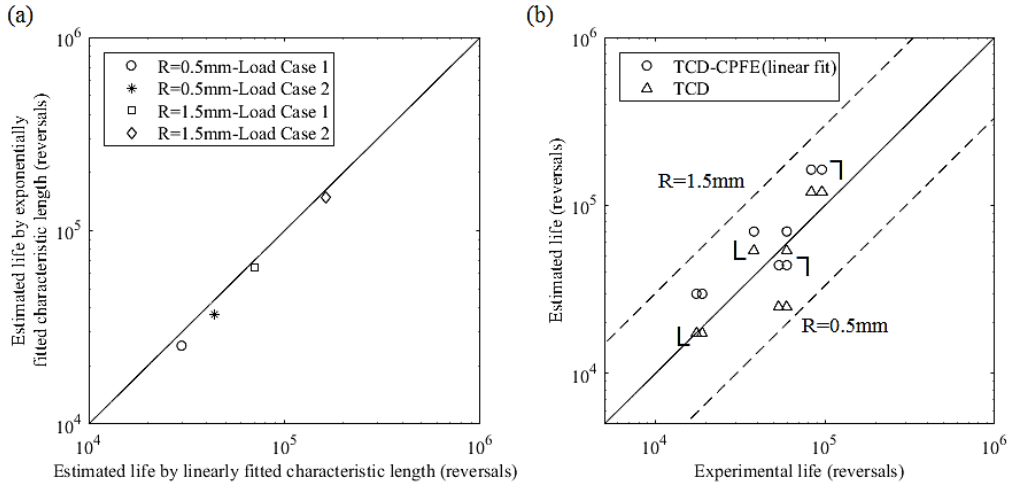

Figure 5.2: (a) A comparison of fatigue lives, estimated by L_{PM}^{CP} and approximated by linearlly and exponentially fitted lines through CPFE results. (b) Experimental fatigue lives versus lives estimated by the TCD-CPFE model

It can be seen from Figure 5.2 that using the CPFE model in order to estimate the material characteristic length of the PM interpretation of the TCD approach for LCF analysis of the material under investigation resulted in life calculations which all fell into the *full acceptance* boundaries. In both configurations, with different notch radii, the fatigue life estimations tended to increase when the TCD was coupled with a CPFE model. This improved the overall life estimations of specimens with R = 0.5 mm but shifted the lives more to the non-conservative side in the case of specimens where R = 1.5 mm. The change is, however, negligible and it also gets smaller if the lives obtained by the exponential line fittings are used.

6 Summary and conclusions

The design and fabrication of components made of high-strength steels require precautions as the intrinsic nature and properties of this type of material make them sensitive to geometrical discontinuities and defects, such as notches, which are inevitable in real applications. In addition, being exposed to cyclic loading conditions makes them susceptible to fatigue failure, which with the presence of notches can significantly degrade their promising performance, which benefits from their high strength. Given these conditions, extensive experimental and analytical investigations are necessary in order to provide data in order to be added to the design and manufacturing guidelines which lack recommendations regarding components made of high-strength and ultra-high-strength steels.

In the current study, a direct-quenched high-strength steel (S960 MC) was investigated under LCF loading by means of experimental and analytical methods in order to characterise the materials properties and obtain the data required for the design phase of components made from this material. Low-cycle fatigue tests under constant amplitude loading were performed on plain and notched specimens, along with analytical notch fatigue analyses.

The material showed cyclic softening (due to the rearrangement of the prestrain-induced dislocations), which was highly pronounced during the first load cycles. The strain-life fatigue curve obtained from experiments was used as a reference curve in order to assess the ability of other approximations (proposed in the published literature) to estimate this curve without the trouble of conducting costly and time-consuming fatigue tests. Among these methods, the approximations that used the monotonic properties were quite successful. A new ANN-based model was implemented using a data set that included experimentally gained mechanical properties of 60 low-alloy steels. This proposed model also yielded acceptable strain-life fatigue curve estimation. The model based on CDM, however, showed suitability in the estimation of curves related to the early fatigue crack initiation stages that corresponded to crack sizes that were less than the sizes concerned by practitioners and designers in engineering applications.

The ANN-based model then was extended to welded joints, which confirmed the superiority of the well-trained models in the estimation of SCFs compared to the empirical equations. The proposed models also were able to explicitly take into account the effects of undercuts (in T-fillet welded joints) and axial misalignment (in butt-welded joints) in the calculation of SCFs.

For fatigue analysis of the notched specimens, the most common analytical methods (linear rule, Neuber’s rule and strain energy density methods) and numerical methods (elastoplastic FE methods) were used. In addition, the approach, based on the elastoplastic reformulation of the TCD, was also utilized (in its PM interpretation), which confirmed the higher accuracy of this method compared with the conventional FE method. In this regard, this method was coupled with the concept of crystal plasticity in

order scrutinize the effect of introducing the microstructural heterogeneity into the calculation of the TCD's material characteristic length and the consequent effect on LCF life estimations. It was interesting to find that a CPFE model can be successfully coupled with the original elastoplastic TCD. This integrated TCD-CPFE model yielded higher values of material characteristic length, which resulted in the trend of less conservative fatigue life estimations for specimens with different notch radii.

Conducting the aforementioned experiments and analyses, two main research goals of the current study were achieved as new results, obtained through extensive tests and measurements, and novelties were achieved through utilizing the mathematical and numerical techniques. However, more studies are definitely required in order to strengthen the reliability of the findings and any recommendations based upon them. Regarding the application of ANN-based models for strain-life fatigue curve estimation and the coupled TCD-CPFE model for notch fatigue analysis, the possible extensions to the current study or aspects requiring further investigation in order to support any concluding remarks are listed as the two following research topics:

- It should be highlighted that the current ANN-based model for the estimation of the strain-life fatigue curve is mainly implemented on the concept of correlation between monotonic properties and experimental fatigue life. Therefore, besides the inherent limitations of the ANN technique for this specific application, uncertainties in the concept itself could act as a source of error in the estimations. A more comprehensive study on a broader range of materials is definitely needed in order to support any conclusion about the applicability of ANN-based models to strain-life curve estimations. It could also be advantageous to perform a sensitivity study such as that conducted by Marohnić & Basan (2016) in order to investigate the level of influence of each monotonic property in the estimation of cyclic properties, as this would lead to a better understanding of how and to what extent the fatigue properties are influenced by the relevant monotonic properties. Such knowledge would be beneficial for the implementation of more robust networks, supplied with the most influential parameters.

- Regarding the TCD-CPFE method proposed for elastoplastic fatigue analysis of notches, a few issues should be further analyzed before making any recommendations based on the findings of the current study with confidence. The results are just reporting the utilization of the TCD-CPFE modelling of round, semi-circular notches on a direct-quenched high-strength steel (S960 MC). Different geometries and notch configurations have to be investigated (as in those already conducted to evaluate the TCD approach in its original form) in order to verify the current results. In addition, the same procedures should be performed on different types of steel (or other metallic materials) in order to test whether the same trend observed here is also true for other materials. In addition to the consideration of other engineering metals and notch configurations, another extension could be the introduction of realistic grain morphologies. This

could be handled by utilizing more complex approaches, such as those proposed by Li et al. (2015), using a novel, generalized method of Voronoi Tessellation in order to generate synthetic, semi-realistic three-dimensional microstructural FE models (even of irregular geometries) that are capable of effectively reproducing and controlling the grain size distribution and grain aspect ratio obtained from experiments.

References

Ban, H. & Shi, G., 2018. A review of research on high-strength steel structures. *Proceedings of the Institution of Civil Engineers - Structures and Buildings*, 171(8), pp. 625–641.

Basan, R., 2017. MATDAT Material Properties Database, http://www.matdat.com/.

Basan, R., Franulovic´, M., Prebil, I. & Črnjarić-Žic, N., 2011. Analysis of strain-life fatigue parameters and behaviour of different groups of metallic materials. *International Journal of Fatigue*, 33(3), pp. 484–491.

Basan, R., Rubeša, D., Franulović, M. & Križan, B., 2010. A novel approach to the estimation of strain life fatigue parameters. *Procedia Engineering*, 2(1), pp. 417–426.

Bäumel, A., Seeger, T. & Boller, C., 1990. Materials Data for Cyclic Loading: Supplement 1. Amsterdam: Elsevier.

Bennantine, J., Comer, J. & Handrock, J., 1990. Fundamentals of Metal Fatigue Analysis. Prentice Hall.

Bhattacharya, B. & Ellingwood, B., 1998. Continuum damage mechanics analysis of fatigue crack initiation. *International Journal of Fatigue*, 20(9), pp. 631–639.

Bhattacharya, B. & Ellingwood, B., 1999. A new CDM-based approach to structural deterioration. *International Journal of Solids and Structures*, 36(12), pp. 1757–1779.

Brennan, F. P., Peleties, P. & Hellier, A. K., 2000. Predicting weld toe stress concentration factors for T and skewed T-joint plate connections. *International Journal of Fatigue*, 22(7), pp. 573–584.

Buch, A., 1984. Notch-size effect in fatigue of steel specimens – verification of some calculation methods. *Materials Science & Engineering Technology*, 15(10), pp. 338–348.

Cailletaud, G. & Pilvin, P., 1994. Utilisation de modèles polycristallins pour le calcul par éléments finis. *Revue Européenne des Éléments Finis*, 3(4), pp. 515–541.

Chen, L. et al., 2014. Processing, microstructures and mechanical properties of ultra-high strength steel sheet. *Procedia Engineering*, 81, pp. 84–89.

Ciavarella, M. & Meneghetti, G., 2004. On fatigue limit in the presence of notches: classical vs. recent unified formulations. *International Journal of Fatigue*, 26(3), pp. 289–298.

Coffin, L., 1954. A study of the effects of cyclic thermal stresses on a ductile metal. *Transactions of ASME*, 76, pp. 931–950.

E606, A., 2013. Standard test method for strain-controlled fatigue testing, West Conshohocken: American Society for Testing and Materials.

E8/E8M, A., 2011. Standard Test Methods for Tension Testing of Metallic Materials, West Conshohocken: American Society for Materials and Testing.

Fatemi, A., Zeng, Z. & Plaseied, A., 2004. Fatigue behavior and life predictions of notched specimens made of QT and forged microalloyed steels. *International Journal of Fatigue*, 26(6), pp. 663–672.

Fricke, W., 2012. IIW Recommendations for the Fatigue Assessment of Welded Structures by Notch Stress Analysis. Oxford: Woodhead Pub.

Gates, N. & Fatemi, A., 2016. Notch deformation and stress gradient effects in multiaxial fatigue. *Theoretical and Applied Fracture Mechanics*, 84, pp. 3–25.

Genel, K., 2004. Application of artificial neural network for predicting strain-life fatigue properties of steels on the basis of tensile tests. *International Journal of Fatigue*, 26(10), pp. 1027–1035.

Hellier, A., Brennan, F. & Carr, D., 2014. Weld toe SCF and stress distribution parametric equations for tension (membrane) loading. *Advanced Materials Research*, 891–892, pp. 1525–1530.

Kiyak, Y., Madia, M. & Zerbst, U., 2016. Extended parametric equations for weld toe stress concentration factors and through-thickness stress distributions in butt-welded plates subject to tensile and bending loading. *Welding in the World*, 60, p. 1247–1259.

Kömi, J., Karjalainen, P. & Porter, D., 2016. Direct-quenched structural steels. In: Encyclopedia of Iron, Steel, and Their Alloys. CRC Press, pp. 1109–1125.

Kujawski, D. & C.R. Sree, P., 2014. On deviatoric interpretation of Neuber's rule and the SWT parameter. *Theoretical and Applied Fracture Mechanics*, 71, pp. 44–50.

Lee, K. & Song, J., 2006. Estimation methods for strain-life fatigue properties from hardness. *International Journal of Fatigue*, 28(4), pp. 386–400.

Lemaitre, J., 1992. A Course on Damage Mechanics. Springer.

Lemaitre, J. & Chaboche, J., 1990. Mechanics of Solid Materials. Cambridge: Cambridge University Press.

Levkovitch, V., Sievert, R. & Svendsen, B., 2006. Simulation of deformation and lifetime behavior of a fcc single crystal superalloy at high temperature under low-cycle fatigue loading. *International Journal of Fatigue*, 28(12), pp. 1791–1802.

Li, L., Shen, L. & Proust, G., 2015. Fatigue crack initiation life prediction for aluminium alloy 7075 using crystal plasticity finite element simulations. *Mechanics of Materials*, 81, pp. 84–93.

Li, L., Shen, L. & Proust, G., 2015. Generalised Voronoi tessellation for generating microstructural finite element models with controllable grain-size distributions and grain aspect ratios. *International Journal for Numerical Methods in Engineering*, 103, pp. 144–156.

Mandel, J., 1973. Equations constitutives et directeurs dans les milieux plastiques et viscoplastiques. *International Journal of Solids and Structures*, 9(6), pp. 725–740.

Manson, S., 1954. Behaviour of materials under conditions of thermal stress, Washington, DC.: National Advisory Committee for Aeronautics.

Manson, S., 1965. Fatigue: A complex subject - Some simple approximations. *Experimental Mechanics*, 5(4), pp. 193–226.

Marohnić, T. & Basan, R., 2016. Study of monotonic properties' relevance for estimation of cyclic yield stress and Ramberg-Osgood parameters of steels. *Journal of Materials Engineering and Performance*, 25(11), pp. 4812–4823.

Meggiolaro, M. & Castro, J., 2004. Statistical evaluation of strain-life fatigue crack initiation predictions. *International Journal of Fatigue*, 26(5), pp. 463–476.

Mitchell, M., Socie, D. & Caulfield, E., 1977. Fundamentals of modern fatigue analysis, Fracture Control Program (No. 26), University of Illinois.

Molski, K. & Glinka, G., 1981. A method of elastic-plastic stress and strain calculation at a notch root. *Materials Science and Engineering*, 50, pp. 93–100.

Muralidharan, U. & Manson, S., 1988. A modified universal slopes equation for estimation of fatigue characteristics of metals. *Journal of Engineering Materials and Technology*, 110(1), pp. 55–58.

Musinski, W. & McDowell, D., 2012. Microstructure-sensitive probabilistic modeling of HCF crack initiation and early crack growth in Ni-base superalloy IN100 notched components. *International Journal of Fatigue*, 37, pp. 41–53.

Neuber, H., 1958. Theory on Notch Stresses. Berlin: Springer.

Ong, J., 1993. An improved technique for the prediction of axial fatigue life from tensile data. *International Journal of Fatigue*, 15(3), pp. 213–219.

Park, J. & Song, J., 1995. Detailed evaluation of methods for estimation of fatigue properties. *International Journal of Fatigue*, 17(5), pp. 365–373.

Park, J. & Song, J., 2003. New estimation method of fatigue properties of aluminum alloys. *Journal of Engineering Materials and Technology*, 125(2), pp. 208–214.

Pavlina, E. & Van Tyne, C., 2008. Correlation of yield strength and tensile strength with hardness for steels. *Journal of Materials Engineering and Performance*, 17(6), pp. 888–893.

Peterson, R., 1959. Notch Sensitivity. In: Metal Fatigue. New York: McGraw Hill, pp. 293–306.

Pleune, T. & Chopra, O., 2000. Using artificial neural networks to predict the fatigue life of carbon and low-alloy steels. *Nuclear Engineering and Design*, 197(1–2), pp. 1–12.

Pujol, J. & Pinto, J., 2011. A neural network approach to fatigue life prediction. *International journal of fatigue*, 33(3), pp. 313–322.

Roessle, M. & Fatemi, A., 2000. Strain-controlled fatigue properties of steels and some simple approximations. *International Journal of Fatigue*, 22(6), pp. 495–511.

Schalkoff, R., 1997. Artificial Neural Networks. McGraw Hill College.

Smith, K., Watson, P. & Topper, T., 1970. A stress-strain function for the fatigue of metals. *Journal of Materials*, 5(4), pp. 767–778.

Srinivasan, V., 2003. Low cycle fatigue and creep–fatigue interaction behavior of 316L(N) stainless steel and life prediction by artificial neural network approach. *International Journal of Fatigue*, 25(12), pp. 1327–1338.

Susmel, L., 2008. The theory of critical distances: a review of its applications in fatigue. *Engineering Fracture Mechanics*, 75(7), pp. 1706–1724.

Susmel, L. & Taylor, D., 2003. Fatigue design in the presence of stress concentrations. *The Journal of Strain Analysis for Engineering Design*, 38(5), pp. 443–452.

Susmel, L. & Taylor, D., 2007. A novel formulation of the theory of critical distances to estimate lifetime of notched components in the medium-cycle fatigue regime. *Fatigue & Fracture of Engineering Materials & Structures*, 30, pp. 567–581.

Susmel, L. & Taylor, D., 2010. An elasto-plastic reformulation of the theory of critical distances to estimate lifetime of notched components failing in the low/medium-cycle fatigue regime. *Journal of Engineering Materials and Technology*, 132(2), pp. 021002-1-8.

Susmel, L. & Taylor, D., 2015. Estimating lifetime of notched components subjected to variable amplitude fatigue loading according to the elastoplastic theory of critical distances. *Journal of Engineering Materials and Technology*, 137, pp. 011008-1-15.

Taylor, D., 2006. The theory of critical distances applied to the Prediction of brittle fracture in metallic materials. *Structural Integrity & Durability*, 1, pp. 145–154.

Taylor, D., 2007. The Theory of Critical Distances: A New Perspective in Fracture Mechanics. London: Elsevier.

Taylor, D., 2016. On the role of microstructure in finite fracture mechanics. Catania.

Taylor, D., Bologna, P. & Bel Knani, K., 2000. Prediction of fatigue failure location on a component using a critical distance method. *International Journal of Fatigue*, 22(9), pp. 735–742.

Upadhyaya, Y. & Sridhara, B., 2012. Fatigue life prediction: A continuum damage mechanics and fracture mechanics. *Materials and Design*, 35, pp. 220–224.

Yoshie, A., Fujioka, M., Onoe, Y. & Okamoto, K., 1992. Effects of rolling and aging conditions on microstructure and mechanical properties of plate steels produced by direct quenching. In: K. G. & R. P., eds. Gilbert R. Speich Symposium Proceedings: Fundamentals of Aging and Tempering in Bainitic and Martensitic Steel Products. Montreal: Proceedings of Gilbert R. Speich Symposium, pp. 119–127.

Zappalorto, M. & Kujawski, D., 2015. Neuber's rules and other solutions: Theoretical differences, formal analogies and energy interpretations. *Theoretical and Applied Fracture Mechanics*, 79, pp. 2–13.

Zipp, R. & Dahlberg, E., 1987. Preparation and Preservation of Fracture Specimens. In: Fractography, ASM Handbook, Vol. 12. American Society for Metals, pp. 72–77.

Appendix I: Fatigue tests results

The results of the fatigue tests based on strain amplitudes and total lives (from P-I).

Table A.1: Fatigue test results

ID	$\Delta\varepsilon/2$ %	Stable or half-life values				E, (MPa)	Life at 50% load drop (cycles)	Total life, N_f (cycles)
		$\Delta\sigma/2$ (MPa)	$\Delta\varepsilon_p/2$ %	$\Delta\varepsilon_e/2$ %	E, (MPa)			
SP 33	1.2002	918.9	0.6744	0.5259	174,597	196,629	373	619
SP 34	1.1989	926.0	0.6901	0.5088	181,475	201,143	339	478
SP 35	1.2001	930.6	0.6825	0.5176	179,456	195,020	356	599
SP 27	0.9978	888.9	0.5055	0.4924	183,599	202,815	640	1,013
SP 28	0.9973	896.6	0.5010	0.4963	182,580	196,505	570	663
SP 30	0.9923	903.3	0.4958	0.4965	180,829	194,807	523	900
SP 11	0.8465	892.7	0.3684	0.4781	188,471	199,882	1,046	1,930
SP 13	0.8487	894.5	0.3814	0.4673	188,299	201,800	832	871
SP 23	0.8446	883.8	0.3523	0.4923	180,202	189,940	976	1,004
SP 1	0.7492	836.8	0.2626	0.4866	173,224	182,329	2,482	3,045
SP 6	0.7685	853.6	0.3086	0.4599	187,411	204,436	2,040	2,910
SP 7	0.7644	847.7	0.2934	0.4710	184,127	196,449	1,866	2,513
SP 2	0.4865	766.8	0.0700	0.4165	183,704	192,251	12,100	13,515
SP 37	0.4972	767.8	0.0819	0.4154	188,284	200,033	8,840	9,122
SP 39	0.4975	790.4	0.0918	0.4058	195,789	196,843	8,110	8,739
				Mean value:	**183,470**	**196,725**		

Appendix II: Materials data

The materials data used in P-II.

Table A.II: The mechanical properties of low-alloy steels, used as a data set in the implementation of the ANN-based model

Material	Designation	σ_u (MPa)	σ_y (MPa)	σ_u/σ_y	RA %	E (GPa)	HV	σ'_f (MPa)	b	ε'_f	c
8 Mn 6	DIN	965	862	1.119	57	198	282	1087	-0.068	0.312	-0.549
8 Mn 6	DIN	869	821	1.058	53	198	282	1073	-0.055	0.203	-0.541
14 Mn 5	DIN	697	580	1.202	68	206	236	1339	-0.111	1.7769	-0.845
22 MnCrNi 3	DIN	1510	1200	1.258	42	198	471	3046	-0.141	0.542	-0.783
23 Mn 4	DIN	1091	1008	1.082	61	207	320	2177	-0.129	0.84	-0.688
25 Mn 3	DIN	540	351	1.538	67	200	140	958	-0.106	0.373	-0.493
25 Mn 5	DIN	1008	904	1.115	49	207	304	1137	-0.069	1.199	-0.74
30 MnCr 5	DIN	950	820	1.159	64	206	309	1482	-0.106	2.7989	-0.824
41 MnCr 3 4	DIN	930	800	1.163	62	207.28	309	1271	-0.082	1.248	-0.653
80 Mn 4	DIN	931	502	1.855	16	187.5	272	1249	-0.101	0.175	-0.451
10 CrMo 9 10	DIN	457	627	0.729	81	210	193	736	-0.065	0.266	-0.527
16 CrMo 54	DIN	556	393	1.415	74	210	164	781	-0.078	0.382	-0.546
30 CrMo 2	DIN	898	780	1.151	67	221	272	1211	-0.071	1.008	-0.652
30 CrMo 2	DIN	1429	1360	1.051	55	200.25	392	1691	-0.08	0.814	-0.674
40 CrMo 4	DIN	940	840	1.119	64	208.78	309	1274	-0.078	1.6739	-0.677
100 Cr 6	DIN	2016	1927	1.046	12	207	560	2620	-0.093	0.145	-0.56
16 NiCrMo 3 2	DIN	981	939	1.045	63	209	319	1010	-0.054	0.9734	-0.693
23 NiCr 4	DIN	808	725	1.114	66	208.531	269	1031	-0.07	0.737	-0.644
40 NiCrMo 7	DIN	1471	1374	1.071	38	193.5	434	1880	-0.086	0.706	-0.662
40 NiCrMo 7	DIN	829	635	1.306	43	193.5	254	1206	-0.095	0.536	-0.568
30 CrMoNiV 5 11	DIN	773	605	1.278	62	212	243	859	-0.059	0.603	-0.62
34 CrMo 4	DIN	1088	1017	1.070	65	193	343	1215	-0.058	0.703	-0.62
34 CrMo 4	DIN	978	893	1.095	67	190	316	1131	-0.061	4.551	-0.848
34 CrMo 4	DIN	1078	980	1.100	61	197	335	1286	-0.063	0.518	-0.594
34 CrMo 4	DIN	881	780	1.129	71	194	283	1160	-0.078	0.65	-0.607
40 NiCrMo 6	DIN	1146	1084	1.057	59	201	357	1360	-0.063	0.32	-0.551
40 NiCrMo 6	DIN	1015	910	1.115	62	190	317	1222	-0.067	0.325	-0.55
40 NiCrMo 6	DIN	1029	953	1.080	62	202	326	1195	-0.061	0.162	-0.467
40 NiCrMo 6	DIN	1067	998	1.069	62	193	338	1274	-0.064	0.612	-0.628
40 NiCrMo 6	DIN	884	810	1.091	67	205	285	1131	-0.072	0.29	-0.54
42 Cr 4	DIN	1006	903	1.114	62	195	318	1212	-0.064	1.2929	-0.716
42 Cr 4	DIN	921	813	1.133	65	194	292	1120	-0.065	0.658	-0.627
42 Cr 4	DIN	952	845	1.127	62	194	305	1252	-0.073	1.294	-0.674
42 Cr 4	DIN	934	833	1.121	65	192	300	1229	-0.072	1.149	-0.667
42 Cr 4	DIN	840	717	1.172	69	193	273	1055	-0.071	0.458	-0.578
50 CrMo 4	DIN	1086	970	1.120	48.6	205	345	1642	-0.092	1.355	-0.706
26 NiCrMoV 115	DIN	1324	1145	1.156	58	202	402	1889	-0.075	0.51	-0.67
4130	AISI	895	779	1.149	67	220	271	1275	-0.083	0.92	-0.63
4130	AISI	1425	1358	1.049	55	200	386	1695	-0.081	0.89	-0.69
4142	AISI	1060	1048	1.011	29	200	327	1450	-0.1	0.22	-0.51
4142	AISI	1415	1379	1.026	48	205	402	1825	-0.08	0.45	-0.75
4142	AISI	1550	1448	1.070	47	200	423	1895	-0.09	0.5	-0.75
4142	AISI	1760	1586	1.110	42	200	477	2000	-0.08	0.4	-0.73
4142	AISI	1930	1862	1.037	37	200	477	2105	-0.09	0.6	-0.76
4142	AISI	1930	1724	1.119	35	205	504	2170	-0.081	0.09	-0.61
4142	AISI	2035	1896	1.073	20	200	504	2070	-0.082	0.2	-0.77
4142	AISI	2240	1689	1.326	27	205	596	2655	-0.089	0.07	-0.76
4340	AISI	825	634	1.301	43	195	255	1200	-0.095	0.45	-0.54
4340	AISI	1240	1172	1.058	57	195	370	1655	-0.076	0.73	-0.62
4340	AISI	1470	1372	1.071	38	200	433	2000	-0.091	0.48	-0.6

5160	AISI	1670	1531	1.091	42	195	456	1930	-0.071	0.4	-0.57
52100	AISI	2015	1924	1.047	11	205	551	2585	-0.09	0.18	-0.56
9262	AISI	925	455	2.033	14	205	274	1040	-0.071	0.16	-0.47
9262	AISI	1000	786	1.272	33	195	295	1220	-0.073	0.41	-0.6
950C	SAE	565	324	1.744	69	205	150	970	-0.11	0.85	-0.59
950X	SAE	440	345	1.275	65	205	150	625	-0.075	0.35	-0.54
950X	SAE	530	331	1.601	72	205	156	1005	-0.1	0.85	-0.61
950X	SAE	695	656	1.059	68	195	236	1055	-0.08	0.21	-0.53
A538A	Other	1515	1482	1.022	67	185	429	1655	-0.065	0.3	-0.62
RQC-100	Other	930	883	1.053	67	205	305	1240	-0.07	0.66	-0.69

Publication I

Dabiri, M., Isakov, M., Skriko, T. & Björk, T.
Experimental fatigue characterization and elasto-plastic finite element analysis of notched specimens made of direct-quenched ultra-high-strength steel

Reprinted with permission from
Proceedings of the Institution of Mechanical Engineers, Part C: Journal of Mechanical Engineering Science
Vol. 231(22), pp. 4209–4226, 2017

Publication II

Dabiri, M., Ghafouri, M., Rohani Raftar H. R. & Björk, T.
Evaluation of strain-life fatigue curve estimation methods and their application to a direct-quenched high-strength steel

Reprinted with permission from
Journal of Materials Engineering and Performance
Vol. 27(3), pp. 1058–1072, 2018

Publication III

Dabiri, M., Ghafouri, M., Rohani Raftar H. R. & Björk, T.
Neural network-based assessment of stress concentration factor in a T-welded joint

Reprinted with permission from
Journal of Constructional Steel Research
Vol. 128, pp. 567–578, 2017

Publication IV

Dabiri, M., Ghafouri, M., Rohani Raftar H. R. & Björk, T.
Utilizing artificial neural networks for stress concentration factor calculation in butt welds

Reprinted with permission from
Journal of Constructional Steel Research
Vol. 138, pp. 488–498, 2017

Publication V

Dabiri, M., Lindroos, M., Andersson, T., Afkhami, S., Laukkanen, A. & Björk, T.
Utilizing the theory of critical distances in conjunction with crystal plasticity for low-cycle notch fatigue analysis of S960 MC high-strength steel

Reprinted with permission from
International Journal of Fatigue
Vol. 117, pp. 257–273, 2018

ACTA UNIVERSITATIS LAPPEENRANTAENSIS

769. JUKKA, MINNA. Perceptions of international buyer-supplier relational exchange. 2017. Diss.

770. BAYGILDINA, ELVIRA. Thermal load analysis and monitoring of doubly-fed wind power converters in low wind speed conditions. 2017. Diss.

771. STADE, SAM. Examination of the compaction of ultrafiltration membranes with ultrasonic time-domain reflectometry. 2017. Diss.

772. KOZLOVA, MARIIA. Analyzing the effects of a renewable energy support mechanism on investments under uncertainty: case of Russia. 2017. Diss.

773. KURAMA, ONESFOLE. Similarity based classification methods with different aggregation operators. 2017. Diss.

774. LYYTIKÄINEN, KATJA. Removal of xylan from birch kraft pulps and the effect of its removal on fiber properties, colloidal interactions and retention in papermaking. 2017. Diss.

775. GAFUROV, SALIMZHAN. Theoretical and experimental analysis of dynamic loading of a two-stage aircraft engine fuel pump and methods for its decreasing. 2017. Diss.

776. KULESHOV, DMITRII. Modelling the operation of short-term electricity market in Russia. 2017. Diss.

777. SAARI, JUSSI. Improving the effectiveness and profitability of thermal conversion of biomass. 2017. Diss.

778. ZHAO, FEIPING. Cross-linked chitosan and β-cyclodextrin as functional adsorbents in water treatment. 2017. Diss.

779. KORHONEN, ILKKA. Mobile sensor for measurements inside combustion chamber – preliminary study. 2017. Diss.

780. SIKIÖ, PÄIVI. Dynamical tree models for high Reynolds number turbulence applied in fluid-solid systems of 1D-space and time. 2017. Diss.

781. ROMANENKO, ALEKSEI. Study of inverter-induced bearing damage monitoring in variable-speed-driven motor systems. 2017. Diss.

782. SIPILÄ, JENNI. The many faces of ambivalence in the decision-making process. 2017. Diss.

783. HAN, MEI. Hydrodynamics and mass transfer in airlift bioreactors; experimental and numerical simulation analysis. 2017. Diss.

784. ESCALANTE, JOHN BRUZZO. Dynamic simulation of cross-country skiing. 2017. Diss.

785. NOKKA, JARKKO. Energy efficiency analyses of hybrid non-road mobile machinery by real-time virtual prototyping. 2018. Diss.

786. VUORIO, ANNA. Opportunity-specific entrepreneurial intentions in sustainable entrepreneurship. 2018. Diss.

787. PULKKINEN, AKI. Towards a better understanding of activity and selectivity trends involving K and O adsorption on selected metal surfaces. 2017. Diss.

788. ZHAO, WENLONG. Reliability based research on design, analysis and control of the remote handling maintenance system for fusion reactor. 2018. Diss.

789. IAKOVLEVA, EVGENIA. Novel sorbents from low-cost materials for water treatment. 2018. Diss.

790. KEDZIORA, DAMIAN. Service offshoring industry: systems engineering approach to its transitional challenges. 2018. Diss.

791. WU, JING. Soft computing methods for performance improvement of EAMA robot in fusion reactor application. 2018. Diss.

792. VOSTATEK, PAVEL. Blood vessel segmentation in the analysis of retinal and diaphragm images. 2018. Diss.

793. AJO, PETRI. Hydroxyl radical behavior in water treatment with gas-phase pulsed corona discharge. 2018. Diss.

794. BANAEIANJAHROMI, NEGIN. On the role of enterprise architecture in enterprise integration. 2018. Diss.

795. HASHEELA-MUFETI, VICTORIA TULIVAYE. Empirical studies on the adoption and implementation of ERP in SMEs in developing countries. 2018. Diss.

796. JANHUNEN, SARI. Determinants of the local acceptability of wind power in Finland. 2018. Diss.

797. TEPLOV, ROMAN. A holistic approach to measuring open innovation: contribution to theory development. 2018. Diss.

798. ALBATS, EKATERINA. Facilitating university-industry collaboration with a multi-level stakeholder perspective. 2018. Diss.

799. TURA, NINA. Value creation for sustainability-oriented innovations: challenges and supporting methods. 2018. Diss.

800. TALIKKA, MARJA. Recognizing required changes to higher education engineering programs' information literacy education as a consequence of research problems becoming more complex. 2018. Diss.

801. MATTSSON, ALEKSI. Design of customer-end converter systems for low voltage DC distribution from a life cycle cost perspective. 2018. Diss.

802. JÄRVI, HENNA. Customer engagement, a friend or a foe? Investigating the relationship between customer engagement and value co-destruction. 2018. Diss.

803. DABROWSKA, JUSTYNA. Organizing for open innovation: adding the human element. 2018. Diss.

804. TIAINEN, JONNA. Losses in low-Reynolds-number centrifugal compressors. 2018. Diss.

805. GYASI, EMMANUEL AFRANE. On adaptive intelligent welding: Technique feasibility in weld quality assurance for advanced steels. 2018. Diss.

806. PROSKURINA, SVETLANA. International trade in biomass for energy production: The local and global context. 2018. Diss.

Acta Universitatis
Lappeenrantaensis
807

LUT University

ISBN 978-952-335-257-5
ISBN 978-952-335-258-2 (PDF)
ISSN-L 1456-4491
ISSN 1456-4491
Lappeenranta 2018